NASCTN Report 4
NTIA Technical Report TR-18-528
NIST Technical Note TN 1980

Measured Emission Spectra of Selected AWS-3 LTE Transmitters

Michael Frey
Geoffrey Sanders
Jolene Splett
John Ladbury
Frank Sanders
Azizollah Kord
Ryan Jacobs

December 2017

NASCTN

National Advanced Spectrum and Communications Test Network

This document is disseminated by the National Advanced Spectrum and Communications Test Network in the interest of information exchange. The United States Government assumes no liability for the contents or use thereof. The United States Government does not endorse products or manufacturers. Trade or manufacturers' names appear herein solely because they are considered essential to the objective of this report.

National Advanced Spectrum and Communications Test Network (NASCTN)

The mission of the National Advanced Spectrum and Communications Test Network (NASCTN) is to provide, through its members, robust test processes and validated measurement data necessary to develop, evaluate and deploy spectrum sharing technologies that can increase access to the spectrum by both federal agencies and non-federal spectrum users.

NASCTN was formed to provide a single focal point for engaging industry, academia, and other government agencies on advanced spectrum technologies, including testing, measurement, validation, and conformity assessment. The National Institute of Standards and Technology (NIST) hosts the NASCTN capability at the Department of Commerce Boulder Laboratories in Boulder, Colorado.

NASCTN is a membership organization under a charter agreement. Members

- Make available, in accordance with their organization's rules policies and regulations, engineering capabilities and test facilities, with typical consideration for cost
- Coordinate their efforts to identify, develop and test spectrum sharing ideas, concepts and technology to support the goal of advancing more efficient and effective spectrum sharing
- Make available information related to spectrum sharing, considering requirements for the protection of intellectual property, national security, and other organizational controls, and, to the maximum extent possible, allow the publication of NASCTN test results
- Ensure all spectrum sharing efforts are identified to other interested members

Current charter members are:

- National Telecommunications and Information Administration (NTIA)
- NIST
- Department of Defense Chief Information Officer (DoD CIO)

NASCTN Report 4
NTIA Technical Report TR-18-528
NIST Technical Note TN 1980

Measured Emission Spectra of Selected AWS-3 LTE Transmitters

Michael Frey
NIST
Geoffrey Sanders
ITS
Jolene Splett
NIST
John Ladbury
NIST
Frank Sanders
ITS
Azizollah Kord
NIST
Ryan Jacobs
NIST

December 2017

Table of Contents

List of Figures

List of Tables

Preface

This test report describes work that was sponsored by the US Air Force. It provides the results of a National Advanced Spectrum and Communications Test Network (NASCTN) campaign to collect Out of Band (OoB) and spurious emissions from Long Term Evolution (LTE) evolved Node B (eNB) and User Equipment (UE) operating in the Advanced Wireless Services (AWS)-3 band. The results of this campaign support electromagnetic compatibility (EMC) analyses for services operating in bands adjacent to AWS-3.

Executive Summary

Version three of Advanced Wireless Services (AWS-3) radio systems is planned to operate at frequencies adjacent to spectral bands currently used by airborne telemetry links at U.S. government test and training ranges. Out-of-band (OoB) and spurious emissions from AWS-3 base stations (called evolved Node Bs, or eNBs) and their associated user equipment (UE) handsets may possibly interfere with these incumbent telemetry receivers. Electromagnetic interference analyses to address this concern depend on knowledge of the power spectra of the AWS-3 eNBs and UE handsets in the frequencies used by these incumbent systems.

The AWS-3 experiments undertaken in this investigation involved spectral measurements of both eNB and UE handset transmitters with different resolution bandwidths, transmitter modulations, resource loadings (number of resource blocks assigned), and handset models for two measurement detector modes. The key findings from these spectral measurements are:

- AWS-3 eNB and UE handset RMS power spectral densities were measured to be down 90-100 dB (at least) from the AWS-3 fundamental frequency in the telemetry bands adjacent to the AWS-3 bands.
- AWS-3 transmitter peak powers are about 10 dB above RMS average powers.
- AWS-3 OoB emissions are insensitive to both modulation scheme (AWS-3 supports quadrature phase shift keying (QPSK), 16 quadrature amplitude modulation (QAM), and 64QAM) and resource block allocation.
- The UE handset experiment involved three UE handsets, two of model A and one of model B. Spectral measurements in this experiment show that the power spectra of different model handsets can vary, presenting the possibility that other/future handset models may exhibit power spectra at some variance with those measured for models A and B.

The above findings directly factor into electromagnetic compatibility analyses for AWS-3 transmitters operating in proximity to test and training range telemetry receivers.

The experiments in this investigation yielded spectral measurements over more than 200 MHz with over 100 dB of dynamic range and uncertainties estimated to be 1–2 dB. This was efficiently accomplished by a combination of filter off-tuning, automated adaptive power attenuation, left/right frequency scanning, and sandwiched calibration. This combination of measurement techniques is recommended for consideration for future studies of transmitter OoB emissions.

Measured Emission Spectra of Selected AWS-3 LTE Transmitters

Michael Frey,[1] Geoffrey Sanders,[2] Jolene Splett,[3] John Ladbury,[4] Frank Sanders,[5] Azizollah Kord,[6] and Ryan Jacobs[7]

Abstract: Version three of Advanced Wireless Services (AWS-3) radio systems will soon use spectrum that is adjacent to bands currently used by airborne telemetry links at U.S. government test and training ranges (TTRs). Spectrum sharing analyses need to be performed to determined how much off-tuning (number of megahertz) and distance separation (number of kilometers) are needed between AWS-3 transmitters and telemetry receiver stations to avoid harmful interference to those receivers. To complete these studies, detailed wide dynamic range emission spectrum measurements of representative models of the soon-to-be-deployed AWS-3 transmitters have been performed. This report describes those measurements, and the method used to obtain them. These measurements have been performed with over 100 decibels (dB) of dynamic range. The measurements have been collected in a variety of resolution bandwidths, transmitter modulations, and types of transmitter loading (i.e., number of resource blocks used) for two measurement detector modes. In general, AWS-3 eNB and UE transmitted emission spectra are found to be insensitive to variations in transmitter configurations. The measured power spectra of the eNBs and UEs vary in direct proportion to measurement (or receiver) bandwidth (i.e., as 10 log measurement bandwidth) with an approximate offset of about 10 dB between peak and average levels. The measurement results indicate that AWS-3 eNB and UE power spectra are suppressed by at least 100 dB in the adjacent telemetry bands for the devices tested. These results can now be factored into EMC analyses for AWS-3 transmitters operating in proximity to telemetry receivers.

Keywords: 1755-1780 MHz; 2155 – 2180 MHz; AWS-3; aeronautical mobile telemetry (AMT); Band 66; band sharing; band sharing analysis; emission spectrum; eNodeB (eNB); interference analysis; out of band (OoB) emissions; spectrum measurements; spectrum sharing; telemetry links; user equipment (UE)

[1] The author is with the National Institute for Standards and Technology, in Boulder, CO.
[2] The author is with the National Telecommunications and Information Administration, Institute for Telecommunication Sciences, in Boulder, CO.
[3] The author is with the National Institute for Standards and Technology, in Boulder, CO.
[4] The author is with the National Institute for Standards and Technology, in Boulder, CO.
[5] The author is with the National Telecommunications and Information Administration, Institute for Telecommunication Sciences, in Boulder, CO.
[6] The author is with the National Institute for Standards and Technology, in Boulder, CO.
[7] The author is with the National Institute for Standards and Technology, in Boulder, CO.

1. Introduction

The Federal Communications Commission (FCC) has auctioned off and is issuing licenses for the introduction of new radio systems in the 1755–1780 MHz (uplink) and 2155–2180 MHz (downlink) radio spectrum in the United States [1]. These bands are commonly referred to as Advanced Wireless Service Band 3 (AWS-3) or Band 66. Out of band (OoB) emissions from Long Term Evolution (LTE) devices have the potential to impact operation of physically co-located and adjacent-band aeronautical mobile telemetry (AMT) systems that operate in the 1780–1850 MHz (L Band) and 2200–2395 MHz (S Band) frequency bands. The AMT systems were designed to receive telemetry signals in the 1755-1850 MHz. Operating in a compressed band above 1780 MHz increases the risk that AMT receive stations are susceptible to AWS-3 UE OoB emissions. Figure 1 depicts this part of the radio spectrum.

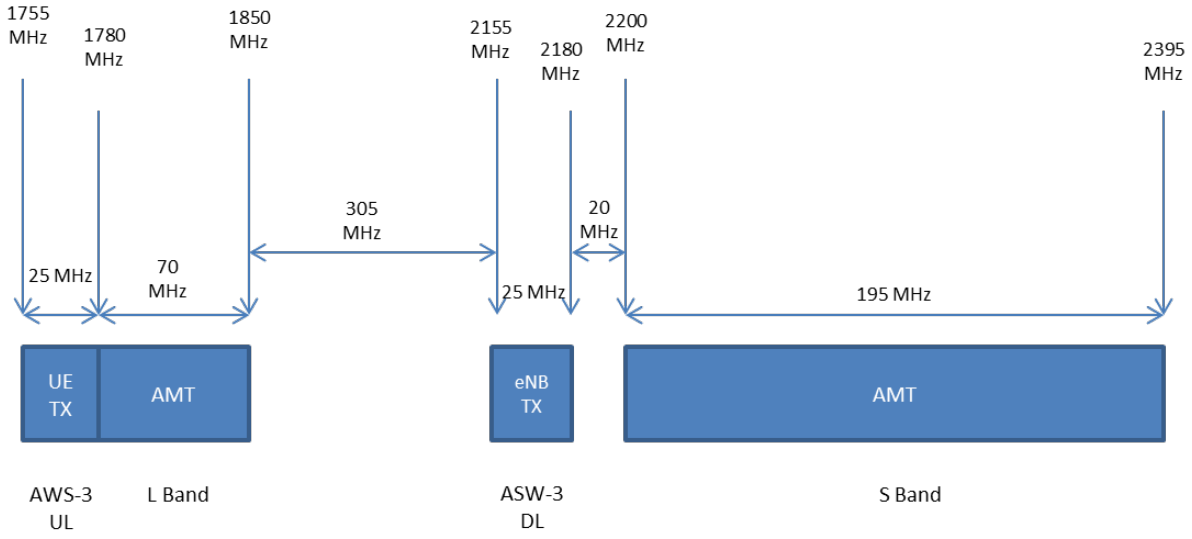

Figure 1. Frequency bands pertinent to these measurements.

A joint team of National Telecommunications and Information Administration (NTIA) and National Institute of Standards and Technology (NIST) engineers have collaborated within the National Advanced Spectrum and Communications Test Network (NASCTN) to perform reproducible, metrology-grade measurements of OoB emissions[8] from selected AWS-3 LTE User Equipment (UEs) and evolved NodeB (eNBs or eNodeB) base stations in the subject AMT bands. The initial investigations and measurements were referred to as Phase I. Because no commercial equipment in the AWS-3 band was available at the beginning of this effort, the Phase I measurements were done on Band 3[9] LTE equipment. The results from Phase I led to a test plan for Phase II. Subsequent Phase II measurements described in this report were executed on AWS-3 LTE equipment.

[8] That is, the OoB emissions of the AWS-3 equipment that are *in-band* to (co-channel with) AMT receiver frequencies.

[9] Band 3 has uplink frequencies of 1710–1785 MHz and downlink frequencies of 1805–1880 MHz.

Spectrum sharing studies require interference analyses that are based on detailed, wide-dynamic-range measurements of emissions from individual transmitters that are to share spectrum with other systems. Such measurements show the rate of "roll-off" of transmitted emissions as a function of off-tuning from transmitter center frequencies. They can show, e.g., that a transmitter's emission levels are reduced by 85 dB relative to the power at the fundamental when a receiver is off-tuned from the fundamental by 73 MHz.

It is sometimes suggested that emission measurements are not needed because it can be assumed that transmitters operate at or near their required emission mask limits. This assumption is nearly always false. Transmitter OoB and spurious emissions are typically lower than emission mask limits, often by tens of decibels [2]. Interference studies that assume transmitter emissions are as high as emission mask limits will therefore overestimate the power spectra of most transmitters' OoB and spurious emissions. As a result, required frequency and distance separations needed for compatible operations between systems will also be overestimated. The only way to avoid such overestimates is to measure accurately the OoB and spurious emission levels of transmitters.

Regarding the new spectrum use that will soon begin in the 1755–1780 MHz and 2155–2180 MHz spectrum, the incumbent adjacent-band systems (Figure 1) are air-to-ground telemetry links that operate at U.S. flight-test ranges. These AMT links use high-gain terrestrial antennas to track airborne platforms carrying telemetry transmitters. The ground-based telemetry antennas feed the airborne platforms' signals into ground-based telemetry receivers for recording and analysis. The new wireless adjacent-band AWS-3 systems anticipated to be introduced at 1.7 and 2.1 GHz spectrum will almost certainly be LTE networks consisting of mobile UE handsets and fixed eNB base stations.

Spectrum sharing analyses need to be performed to determined how much off-tuning (number of megahertz) and distance separation (number of kilometers) are needed between AWS-3 LTE transmitters and AMT receiver stations to avoid harmful interference to the telemetry receivers. To complete these studies, detailed wide dynamic range emission spectrum measurements of representative models of the soon-to-be-deployed AWS-3 transmitters are needed. This report describes such measurements, and the method used to obtain them.

Interference analyses often require emission spectrum measurements with a dynamic range of 100 dB or more. Available measurement instrumentation often does not achieve such wide dynamic ranges, including swept-frequency and high-speed time-domain sampling systems. To overcome this limitation and achieve dynamic ranges of as much as 120 dB in OoB emissions measurements, a measurement system with the characteristics described below needs to be used. The measurements reported here achieved dynamic ranges beyond the standard 3GPP measurements as documented in 3GPP TS 36.101 and 3GPP TS 36.141 ([3], [4]).

Figure 2 shows how the measurements described in this plan can be used in spectrum sharing analyses for mobile-to-telemetry interference scenarios.

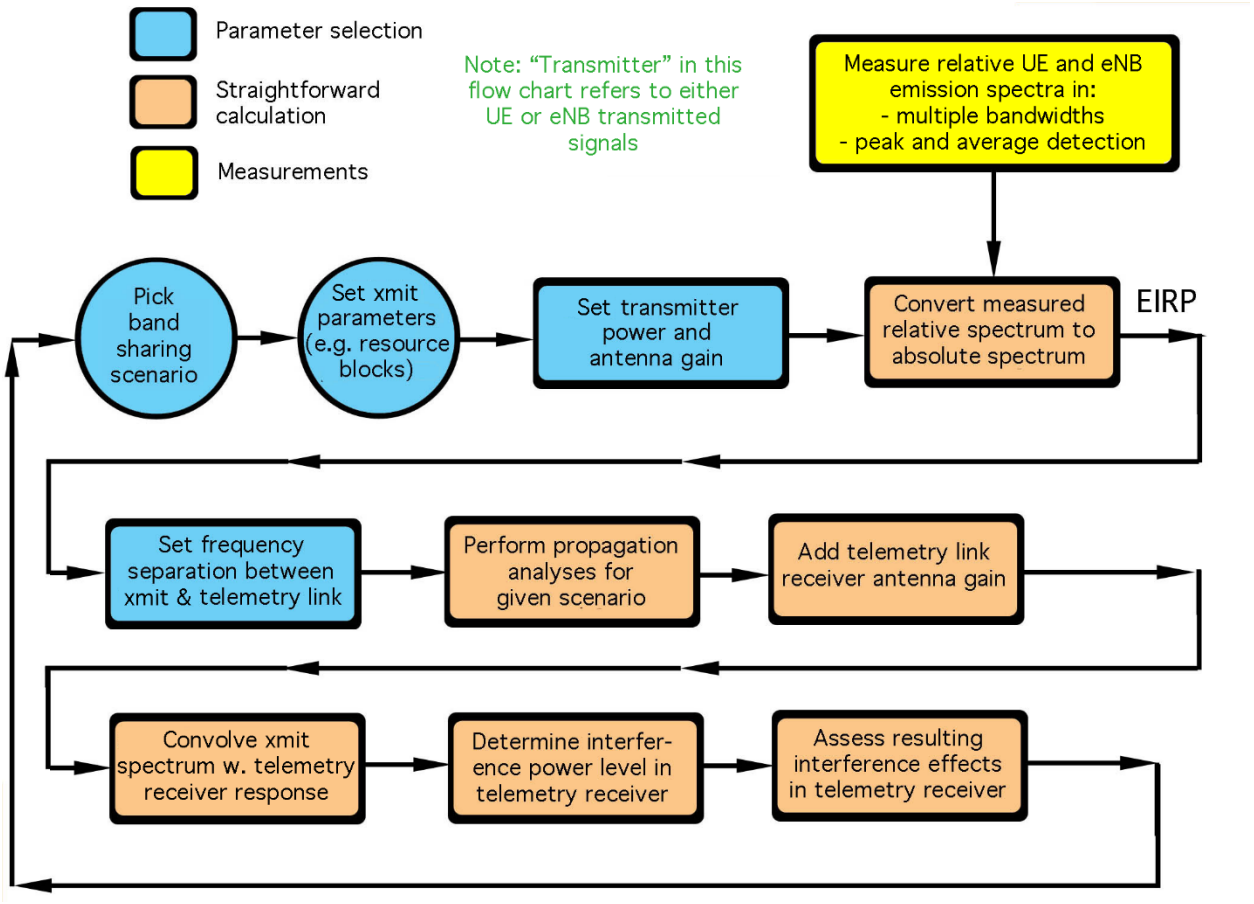

Figure 2. How emission spectrum measurements can be used in AWS-3 band sharing analysis studies.

The measurement system uses a radio frequency (RF) front end with three major components: a variable RF attenuator, a tunable bandpass filter, and a low-noise amplifier (LNA). The RF attenuator extends the dynamic range of the measurement system, the bandpass filter rejects high-power signals when the measurement system is off-tuned from the transmitter fundamental frequency, and the LNA provides a low measurement system noise figure (high sensitivity to weak signals) in low-power portions of the transmitter emission spectrum.

The transmitter power measurements in this study provide a set of emissions data (power spectral densities) for deployed hardware. These data demonstrate the type of emissions that may be observed in AWS-3 and their adjacent bands. This report presents these data and describes the methods of their collection.

1.1. Objective

The objective was to measure transmitter emission spectra of representative AWS-3 UE and eNB transmitters with enough dynamic range to determine their OoB and spurious emission levels in the adjacent telemetry bands. Transmitter factors that were varied to determine effects, if any, on the measured peak and RMS OoB emissions included:

- Measurement bandwidth

- Transmitter modulation mode
- Variation in number and configuration of transmitter resource blocks (RBs)

1.2. Background

The Phase II emission spectrum measurements were performed on AWS-3 hardware in a laboratory setting. The measurement system configurations used in Phase II were based on the results of the Phase I study. Details on the Phase I results are included as an Appendix to the Phase II test plan which can be found at the NASCTN web-site (https://www.nist.gov/communications-technology-laboratory-ctl/nasctn).

The measurement system was connected to the eNB Device Under Test (DUT) via hard-lines (i.e., conducted measurements). UE measurements were completed using a short-range (several cm) radiated path between the UE DUT and a small horn in an anechoic chamber. For all testing, UEs were operated at their maximum output power levels. The eNB was operated in a conducted measurement mode at 100 mW, consistent with the sensitivity of the measurement system front end.

For each DUT, the emission spectrum was measured in peak and average detection modes in bandwidths of 100 kHz, 300 kHz, 1 MHz, and 3 MHz; 1 MHz is the reference bandwidth for all measurements. Emission spectra were measured for a different number of RBs used by the UEs and the eNB. The eNB spectrum was measured for a center-tuned frequency and the UEs were measured at a frequency near the upper end of its operational band.

All measured emission spectra were reported in terms of power relative to the power measured at the transmitters' center frequencies (f_0).

2. DUTs

This measurement effort used consumer-grade AWS-3 LTE hardware. Recognizing the potential for the large number of manufacturers and types of AWS-3 LTE devices, it was not practical to test all AWS-3 UEs and eNBs deployed in the future marketplace, so a subset of available equipment models was selected for testing. Additionally, available AWS-3 equipment at the time of testing limited the number of devices possible for testing.

2.1. AWS-3 UEs

An examination of existing deployments in the current U.S. LTE bands reveals four categories of UE types: mobile handsets (also commonly referred to as smartphones), tablets, consumer premises equipment or consumer provider equipment (CPE), and LTE routers that serve as Wi-Fi access points and then convert traffic to LTE. Examples of CPE are nano/pico/femto-cell base stations that may be deployed inside a dwelling for the purpose of repeating ('boosting') LTE signals.

According to a 2015 study done by a UE manufacturer [5], smartphones constitute about 75% of the North American UE deployments. Given this, this study team decided not to measure the emissions from devices other than LTE UE handsets.

To select from all available UEs, we examined which UEs are most commonly sold in the U.S. (for any band/network). A marketing research firm conducts a quarterly survey [6] of the most commonly sold UEs worldwide by surveying mass market retailers and distributors. The disadvantage of this study is that it does not include sales through wireless carriers. Therefore, we assume that the most popular UE handsets sold through mass-market retailers are very similar (if not identical) to those from carriers.

As an additional constraint, commercial equipment supporting operations in AWS-3 band was in limited supply at the time of testing. This limited the test to three UE handsets, two of the same model from one manufacturer and one from a second manufacturer. Additional testing could be performed as more commercially AWS-3 equipment is available to establish more confidence in the variability of OoB emissions.

A disadvantage of the tested UEs is that they lack accessible hardware RF ports for conducted RF emissions measurements. This issue is now commonly encountered in UEs. Therefore, only coupled/radiated measurements were possible in Phase II. The coupled/radiated measurement method is further discussed in Section 4.

2.2. AWS-3 eNB

For eNB emissions measurements, we only considered macro-cell eNBs. There will almost certainly be small cell deployments in the AWS-3 band, but they will all be at relatively low transmitter power (e.g., less than 1 watt) and most will be deployed indoors. Short of one being deployed in the immediate vicinity of an AMT system, their emissions are not expected to be of significant concern.

Though there are significantly fewer models of eNBs than there are UEs, it was still not practical to test all available models. There are no market sales data available to identify which models or manufacturers of AWS-3 eNBs might eventually be the most popular. In the end, in fact, only a single model of AWS-3 eNB radio was located in all of the United States that could be made available for measurements. This model is referred to in this report as the AWS-3 eNB.

By design, all macro-cell eNBs have hardware RF ports. The conducted measurement method is further discussed in Section 5.

3. Measurement Approach and Equipment

3.1. RF Front End/Preselector

The overall measurement technique was based on the stepped-measurement approach described in the best practices NTIA report [7]. Although the report described the technique as applied to measurements of radar emission spectra, the same technique works equally well for LTE-type emissions, as described for a 3.5 GHz LTE hotspot in [8].

Interference analyses often require emission spectrum measurements with a dynamic range of 100 dB or more. Available measurement instrumentation, including swept-frequency and high-speed time-domain sampling systems, does not achieve such wide dynamic ranges. To overcome this limitation and achieve dynamic ranges of as much as 130 dB in emission measurements, a measurement system with the characteristics described in [7] was used. As shown in Figure 3, the heart of this approach lies in the use of a radio frequency (RF) front end with three major components: a variable RF attenuator, a tunable bandpass filter, and a low-noise amplifier (LNA). The RF attenuator extends the dynamic range of the measurement system, the bandpass filter rejects high-power cellular signals when the measurement system is off-tuned from the cellular fundamental frequency, and the LNA provides a low measurement system noise figure (high sensitivity to weak signals) in low-power portions of the cellular emission spectrum.

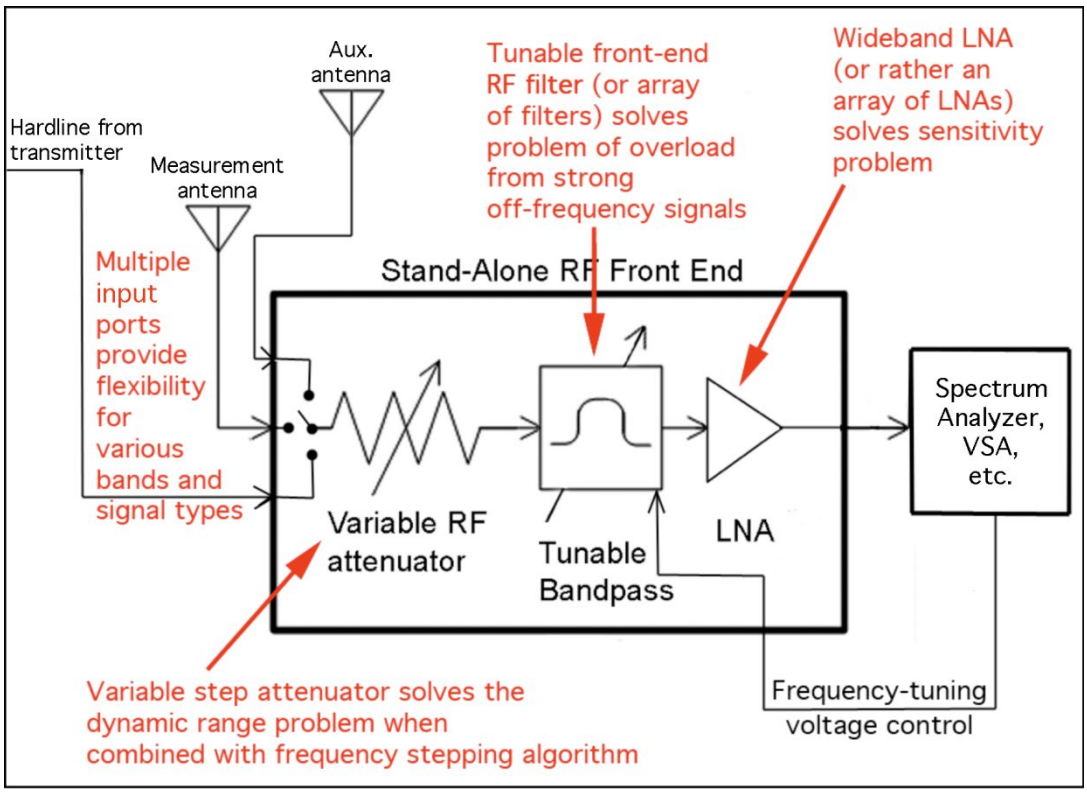

Figure 3. Block diagram of RF front end used for wide dynamic range spectrum measurements.

The key to operating the measurement system is to step across the emission spectrum one frequency at a time. Stepping means tuning the measurement system to a single frequency and then waiting long enough at that frequency for the transmitter (in this case an LTE system) to provide a representative number of samples from which a peak and root mean square (RMS) average power on that frequency may be computed. For LTE transmitters, this interval has been found empirically to be 0.5 seconds or longer. During this effort, a sufficient dwell time was in fact determined during the measurements to be 0.5 seconds. In general, there is no ultimate peak amplitude. The peak response will depend on measurement time, sample rate, and possibly other parameters, with the expected peak amplitude increasing with measurement time and with sample rate. For valid comparisons, a consistent parameter configuration is important.

When a measurement has been completed at a tuned frequency, the measurement system is tuned (stepped) to the next frequency to be measured. The frequency interval between tuning steps is usually (but not necessarily) equal to the resolution bandwidth of the measurement system.

For LTE measurements, the radar process of [7] was adapted as follows. Instead of running the spectrum analyzer solely in peak detection mode, the measurement system was operated in both peak-detection and RMS detection modes.

The peak and RMS measurement process was repeated at each frequency step in the spectrum. The RMS spectrum points were measured as the average of 1001 RMS-detected points (601 points for the UEs) collected over a 0.5 second interval of each measured frequency step. The peak-detected point at each frequency was taken as the maximum measured power level (peak detected) during that interval.

Because stepped-frequency emission spectra are measured a single frequency at a time, the amount of attenuation invoked at the RF front end can be gradually adjusted as the measurement frequency steps progress across the spectrum. Zero attenuation is used in the lowest-power parts of the spectrum, maximum attenuation is used at the transmitter's center frequency and intermediate amounts of attenuation are used at points in between.

3.2. Coffin Corner Effect

The design of equipment used by LTE UEs and eNBs (e.g., amplifiers, filters) result in the DUTs exhibiting steep power drops just a few MHz from the tuned frequency. The steep change, while good for spectrum engineering, is challenging for emission spectrum measurements. The problem is that the center-frequency (f_0) power from the transmitter can still be received in the measurement system through the front-end yttrium-iron-garnet (YIG) filter, even when the measurement system is *not* tuned to f_0; the YIG filter has a finite, non-zero bandwidth. For the measurement system described here, the YIG filter bandwidth is on the order of 25 MHz (although it varies with tuned frequency). The non-zero characteristic means that, if the transmitter's power change with frequency is steep enough, the transmitter will still put enough power into the front end through the YIG filter to either overload the front end LNA or else overload the downstream spectrum analyzer Intermediate Frequency (IF) stage when measurements are being performed close to f_0.

This problem cannot be solved by simply adding attenuation in the RF front end; the added attenuation would push the transmitter's OoB power at the measured frequency below the measurement system's noise floor. Either the measurement system attenuation is kept low enough to allow the transmitter's power on the measurement frequency to be seen, causing the transmitter's f_0 power to overload the measurement system, or the attenuation is made great enough to eliminate the overload condition, causing the transmitter power at the measured frequency to be lost below the measurement system's noise floor. Under these conditions the measurement system's dynamic range drops from a nominal 100+ dB to zero dB. This is the spectrum measurement coffin corner problem [9].

The coffin corner problem eventually occurs whenever the power spectrum changes steeply enough relative to the bandwidth of the RF front-end YIG filter. Ideally, the YIG filter bandwidth would be made narrower, but that is not physically practical as that would introduce unacceptable loss. The YIG filter's bandwidth can, however, be *effectively* narrowed on an ad-hoc basis relative to its frequency separation from f_0. The way to do this is to off-tune the YIG filter as much as possible from the measurement system's tuned frequency. The off-tuning approach is shown graphically in Figure 4. An alternative to the off-tuning approach is a sharp notch filter tuned to remove the high-level signal. However, because our interest is the relative power of the in-band and OoB emissions, a notch filter would involve a more complex set of measurements.

The more the YIG filter can be off-tuned, the better for solving the coffin corner problem. In practice, the off-tuning is limited by the eventual roll-off of the YIG filter's passband shape. The off-tuning is performed up to the 3 dB points in the filter's rejection curve. As shown in Figure 4, the YIG filter off-tuning is downward when the transmitter's spectrum is being measured below f_0, and is tuned upward for the transmitter's spectrum above f_0.

Sometimes the spectrum is so steep that even off-tuning of the YIG filter does not completely solve the problem. But off-tuning of the YIG filter will always greatly reduce the number of frequency points where the coffin corner occurs, usually reducing the number of such points to either zero or else just a few on either side of f_0. YIG filter off-tuning was performed for the eNB and UE measurements, since both demonstrated the coffin corner problem.

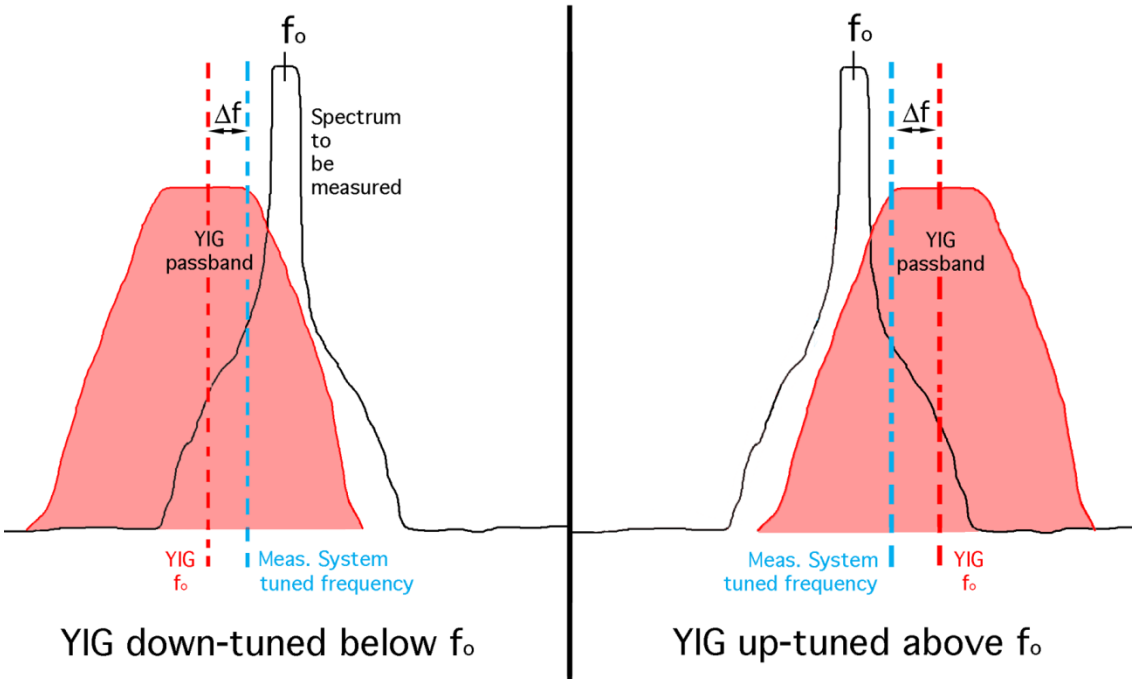

Figure 4. YIG filter off-tuning technique that was used for wide dynamic range eNB emission spectrum measurements. The YIG filter center is offset (Δf) from the measurement system's tuned frequency up to the limit of the YIG filter's 3-dB roll-off points, half of the YIG filter's flat passband width.

3.3. Spectrum Analyzer

The spectrum analyzer used in these measurements was an Agilent (now Keysight Technologies) E4440A.[10] A block diagram of the E4440A is shown in Figure 5.

[10] Any similar spectrum analyzer could be used to replicate the measurements in this report.

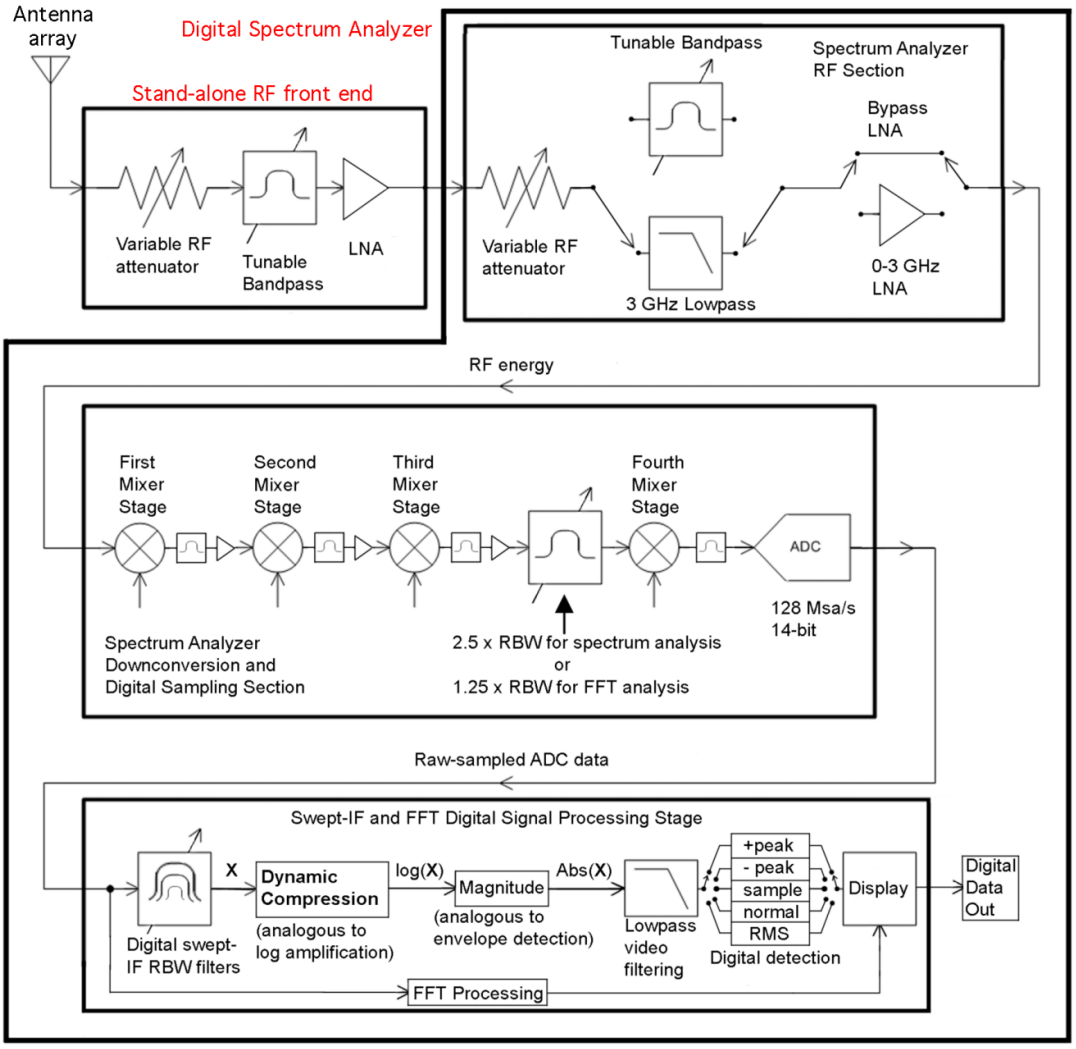

Figure 5. Block diagram of the E4440A digital spectrum analyzer with a stand-alone RF front end, as used for the UE and eNB spectrum measurements.

3.4. eNB (Base Station) Emulator for UE Emission Measurements

UEs will not operate unless they are in communication with eNB base stations. Setting up an eNB for this purpose is impractical so an eNB emulator was used instead. The eNB emulator used in these measurements was a Rohde and Schwarz CMW-500.[11] The CMW-500 is used for communications design verification, feature testing and certification of user equipment (e.g., smartphones and dongles). The CMW-500 is capable of emulating all LTE protocol layers: physical, MAC, RRC, and PDCP, and it is able to force the UE to operate under a specified set of conditions. The CMW-500 was used to set up smartphone UEs to transmit with the carrier frequency and bandwidth of interest in order to measure OoB emissions. The CMW-500 was used to set the emulated UE transmitter power level and used grants to control the RBs that the UEs transmitted within the bandwidth of interest.

[11] Any similar eNB emulator could be used to replicate the measurements in this report.

4. UE Device Measurement

4.1. UE Measurement Setup

Figure 6 shows a block diagram of the UE measurement system. The specialized custom RF front end built by NTIA can be replicated with similar components. The UE devices being measured used Orthogonal Frequency Division Multiplexing (OFDM) modulation and were frequency domain duplexed (FDD) with the CMW-500 emulating an eNB. The CMW-500 parameters during the emission measurements are shown in Table 1.

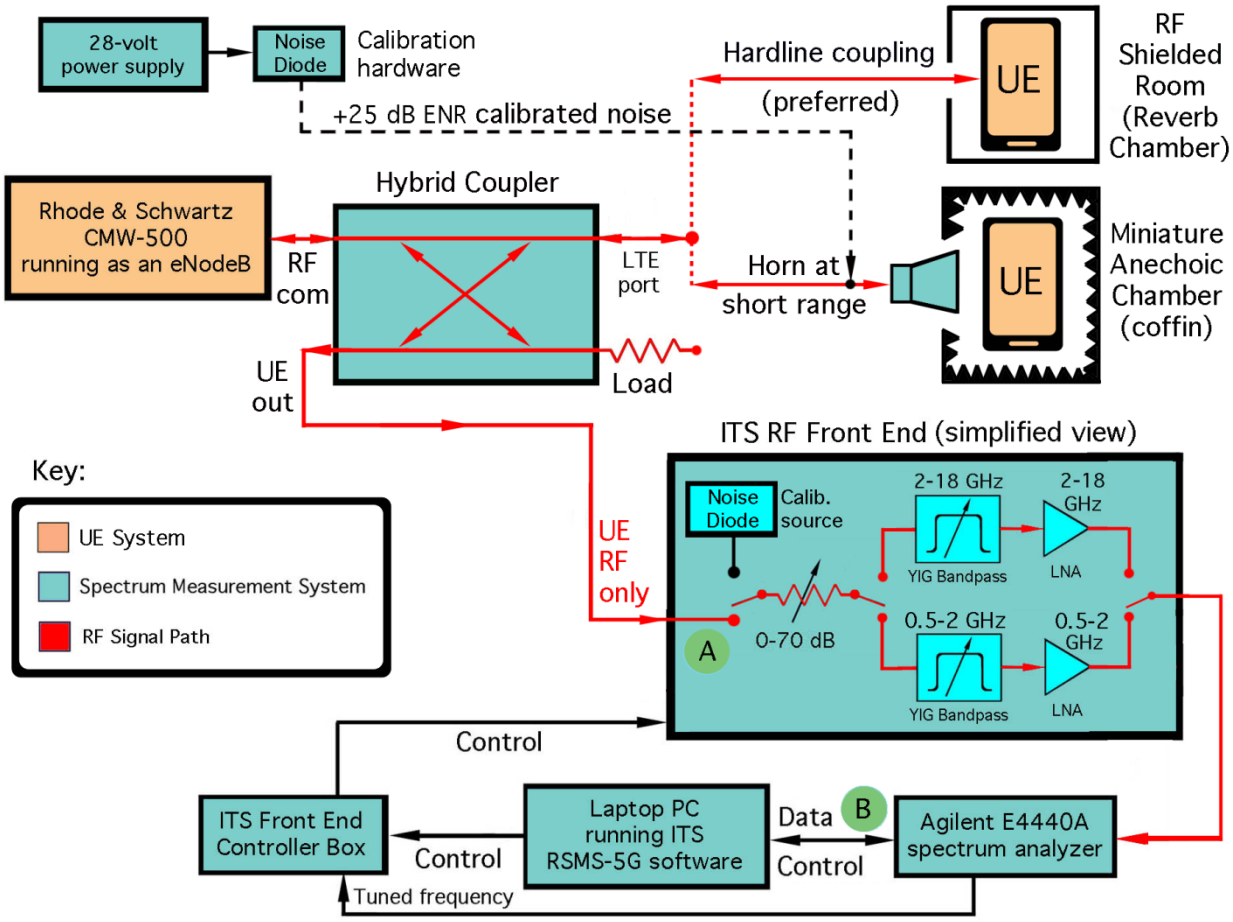

Figure 6. Block diagram of the UE emission spectrum measurement system.

To isolate the DUT UE signal from the CMW-500 eNB signal for the spectrum measurement, the measurement system used a hybrid coupler as a splitter, as shown in Figure 6. The coupler/splitter provided about 20 dB of decoupling. The CMW-500 was operated at the lowest possible power level that still allowed control of each UE being measured; these power levels were determined empirically by the measurement personnel through trial and error. These expedients (coupler/splitter and minimal CMW-500 power) kept the CMW-500 emissions from contaminating the UE emission spectrum measurement results.

The measurement system measured the UE signal from an RF splitter on the UE side of the loop. The measurement system noise figure from the input to the RF front end was approximately 8 dB; the measurement system gain was approximately 24 dB.

Table 1. Operating parameters of the R&S CMW-500 during UE spectrum measurements.

UE Parameter	Parameter Value
Duplexing	Frequency Division (FDD)
RF Modulation	Quadrature Phase Shift Keying (QPSK) 16 Quadrature Amplitude Modulation (QAM)
Operating Radio Band	AWS-3 Band 66 (1755-1780 MHz)
Commanded Full Cell Bandwidth	10.0 MHz
Total Requested Output Power	+23 dBm
Resource Block (RB) Energy Per Resource Element (EPRE)	-100.0 dBm/15 kHz (indicated by eNB emulator)
Full Cell Power	-72.2 dBm (indicated by eNB emulator)
Physical Uplink Shared Channel (PUSCH) Open Loop	+23.0 dBm (indicated by eNB emulator)
PUSCH Closed Loop	+23.0 dBm (indicated by eNB emulator)
Switching	Packet
State	Radio Resource Control (RRC)
Transfer Block Size Index (TBSI) (Downlink)	9
TBSI (Uplink)	6
Start Resource Block	0
Downlink Throughput (50 RBs)	4.795 Mbit/sec
Uplink Throughput (50 RBs)	2.064 Mbit/sec
Protocol	Internet Protocol Version 4

As shown in Figure 6, the preferred method of connecting the UEs to the measurement system was via hardline connections on the phone bodies. This can be a mechanically difficult process, but is possible for some UEs. For other UEs, however, no hardline connection is possible. In this case, the DUT UEs are measured with a dual-ridged horn antenna in a mini-anechoic chamber.

For the measurements of this report, all DUT UEs were radiatively coupled to the measurement system due to their lack of hardline connector points for RF radiation. The measurement engineers moved the UEs around (with respect to the horn's aperture) the measurement horn antenna enough to maximize power coupled into the measurement system horn antenna from each UE. This was important because the more power that gets into the measurement system, the more dynamic range is obtained in the spectrum measurement. In all cases, the relative placement of the UE and the coupler was recorded (including photographically) to document the placement of the units during the measurements. Figures 7 through 10 show images of the UE measurement system.

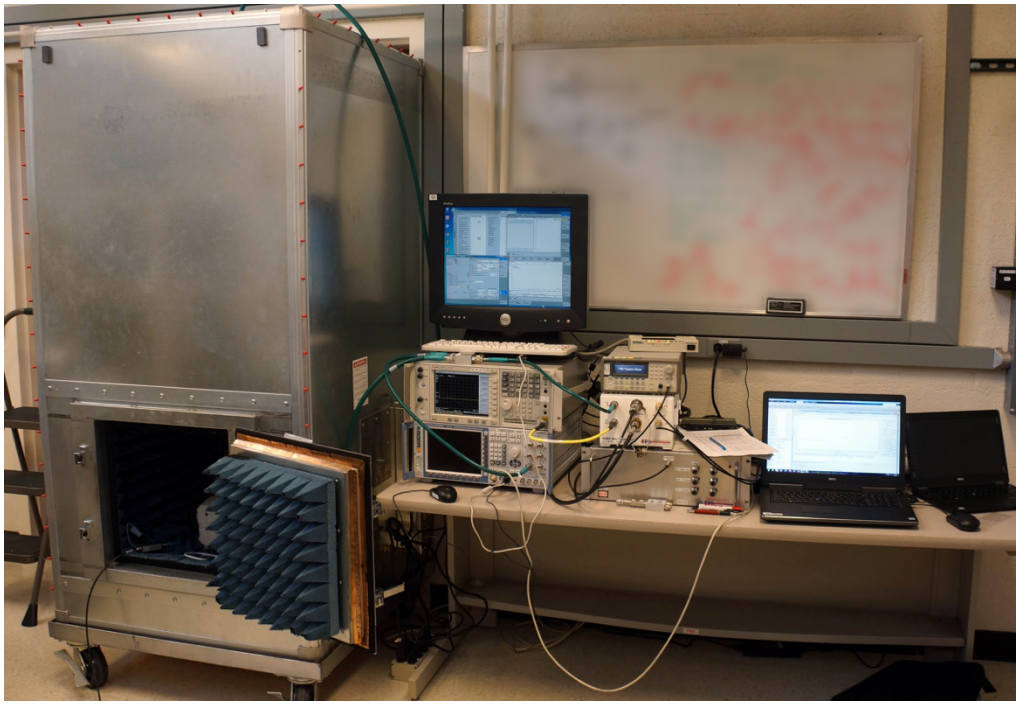

Figure 7. UE measurement system with the anechoic chamber on the left.

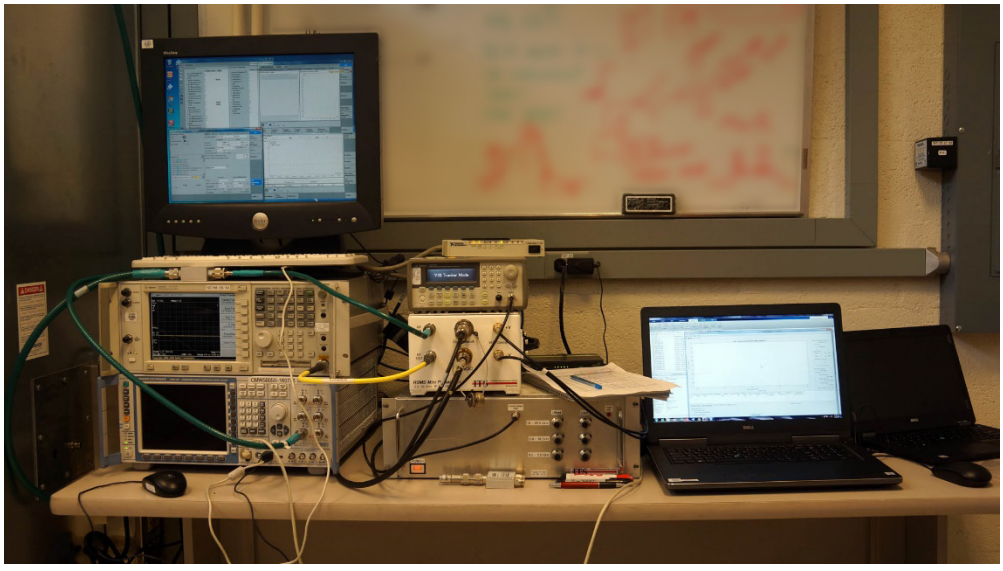

Figure 8. UE measurement system boxes including the CMW-500 (lower left), E4440A (on top of the CMW-500), RF front end (white box at center), RF front end auxiliary boxes (above and below it) and the controller laptop computer (far right).

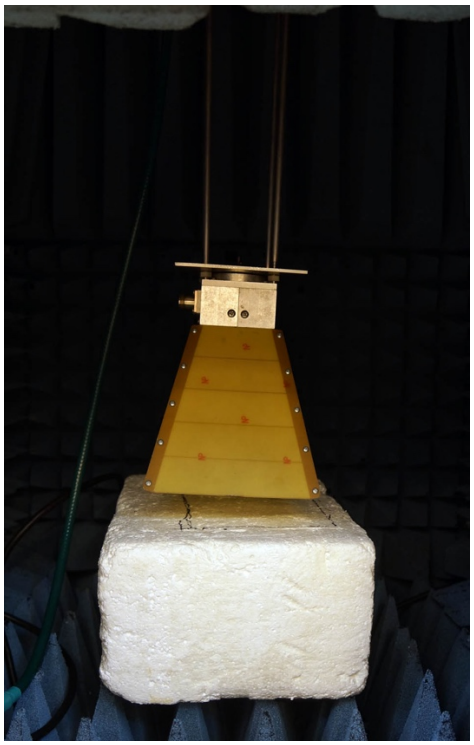

Figure 9. The anechoic chamber interior with the measurement horn antenna suspended above the UE Styrofoam-block stage.

Figure 10. A UE positioned approximately 3 cm underneath the horn antenna during emission measurements.

4.2. UE Measurement Procedure

All measurements were performed on UEs where the UE power was maximized by setting the CMW-500 to request maximum power output power from the UEs. The CMW-500 eNB was operated at the lowest possible power level to reduce the potential for any contamination of the UE measurements.

The relative offsets in measured power between a transmitter's fundamental frequency and its OoB emissions varies as a function of the resolution bandwidth and measurement detector mode. The amount of this variation is ultimately determined by the modulation of the transmitter’s emissions. For noise-like transmitter modulations that are RMS detected, the variation in the receiver power is directly proportional to the width of the resolution bandwidth (RBW) (10log(RBW)). By comparison, for peak-detected pulsed transmitter emissions, this variation tends toward its other extreme, 20log(RBW). For various other modulations and measurement detectors the multiplying factor is some value between these extremes, i.e., between 10 and 20. To characterize this variation in OoB power relative to power at their fundamental frequencies for the transmitters in this study, the transmitters' emissions need to be measured across a range of RBWs.

Using a range of RBWs during the measurements allows the coefficient of the OoB emissions and spurious-to-fundamental power variation (always somewhere between 10 and 20) to be determined. With this variation known, the measurement results can be extrapolated to victim receivers with any given bandwidth, even if victim receiver bandwidths do not necessarily correspond to any actual measurement bandwidth used in this study.

The eNB emulator controlled the number and location of the RBs used by the UE. The team ran several tests varying the location of the RBs used by the UE which showed no significant difference in OoB emissions. The experiment design allocated RBs closest to the ATM band since this represents the worst-case for OoB emissions.

5. eNB Measurement

5.1. eNB Measurement Setup

Figure 11 shows the setup for the eNB measurements. The DUT eNB could be operated stand-alone, without an associated radio to force it to operate.

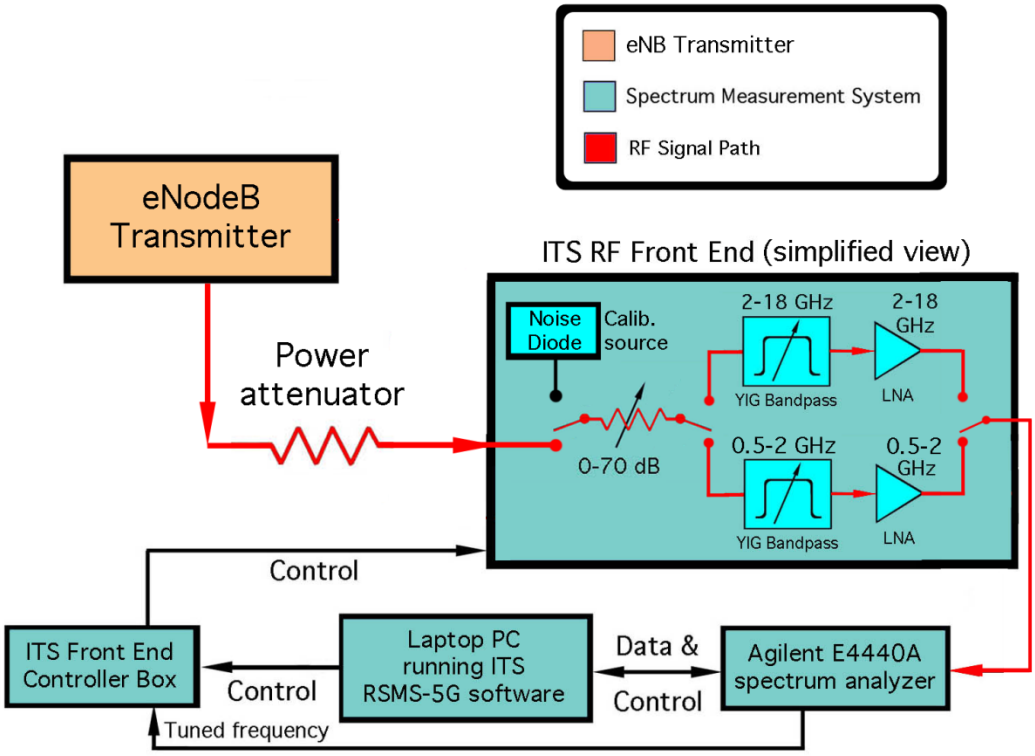

Figure 11. Block diagram of the eNB spectrum measurement system.

5.2. eNB Measurement Procedure

The eNB emission spectra were measured with the transmitter operating at 100 mW with a power attenuator on its output to prevent overload of the measurement system. A picture of the eNB is shown in Figure 12.

eNB emission spectrum measurements showed that the measured power of these spectra can change by 80 dB or more within just a few megahertz of tuned spectrum. The drop-off is likely achieved by a combination of excellent modulation control and high-quality eNB transmitter output filtering.

The relative offsets in measured power between a transmitter's fundamental frequency and its OoB emissions will vary as a function of the RBW and measurement detector mode in the same manner as discussed with the UE measurements in Section 4.2. Using a range of RBWs during the measurements allows the multiplying factor associated with the OoB emissions and spurious-to-fundamental power variation (always somewhere between 10 and 20) to be determined. With

this variation known, the measurement results can be interpolated to victim receivers with any given bandwidth, even if victim receiver bandwidths do not necessarily correspond to any actual measurement bandwidth used in this study.

The allocation of RBs was controlled by the test configuration of the eNB. The test configuration limited the RB allocation to start from the lowest part of the band.

Figure 12. eNB used for measurement.

6. Calibration Procedure

The measurement system was calibrated with noise diodes. The basic approach was classic Y-factor, in which the noise diode is turned on at the front end of the measurement system at a known excess noise ratio[12] (ENR), with a value between 20 and 25 dB for our measurements. Losses between the noise diode and the measurement instrumentation must be kept well below the ENR to keep measurements above the measurement noise floor. The power from the diode is measured for a set of frequencies across the expected frequency range of the ensuing measurements. Then the diode is turned off and the output of the measurement system is measured a second time for each of the calibration frequencies. The power difference between diode = ON and diode = OFF is then computed for each frequency. Those calibration factors are

[12] ENR is relative to *kTB*, where *k* is Boltzmann's constant (1.38^-23 J/K/Hz), *T* is the ambient temperature and *B* is the bandwidth in which the noise is observed or measured.

stored in a frequency-dependent look-up table. They are retrieved and applied (that is, the measurement system's gain corrections are applied) to the measured spectrum data on a point-by-point basis. The calibration factors were interpolated from the look-up table calibration frequencies, when necessary. Measured RF emission spectra are thus calibrated to power occurring at the noise diode calibration point.

As shown in Figure 11, the NTIA front end contains a built-in noise diode, but an external diode can also be used. In fact, for these measurements, the built-in noise diode was used for the eNB measurements and an external noise diode was used for the UE measurements. For both the UE and the eNB measurements the noise diode was attached to the respective measurement systems at the antenna (for the UE work) and at the eNB transmitter output.

7. Statistical Analysis

The data obtained for this study provided a means of comparing different test conditions. In addition, repeated measurements at the various test conditions were used to estimate the uncertainty of a reported spectral power measurement. Uncertainties derived from repeated measurements accounted for many sources of variability that could not be directly controlled or measured. Uncertainty due to environmental conditions and spurious emissions were minimized by carrying out conducted measurements for the eNB and radiated measurements in an anechoic chamber for UEs.

7.1. eNB Experiment Plan

The eNB OoB emissions experiment followed an experiment plan that focused on three experimental factors: resource allocation, modulation scheme, and RBW. Resource allocation and modulation scheme were both considered to potentially significantly affect OoB spectral content. RBW, which reflects the bandwidth of the OoB emissions receiver, was included as a study factor to assess the potential impact of OoB emissions on different receivers. The three factors were varied one-factor-at-a-time in the experiment proceeding from an eNB baseline configuration consisting of a full 50 resource block allocation QPSK transmission at a 2165 MHz center frequency measured with a 1 MHz resolution bandwidth. The eNB experiment plan is shown in Figure 13.

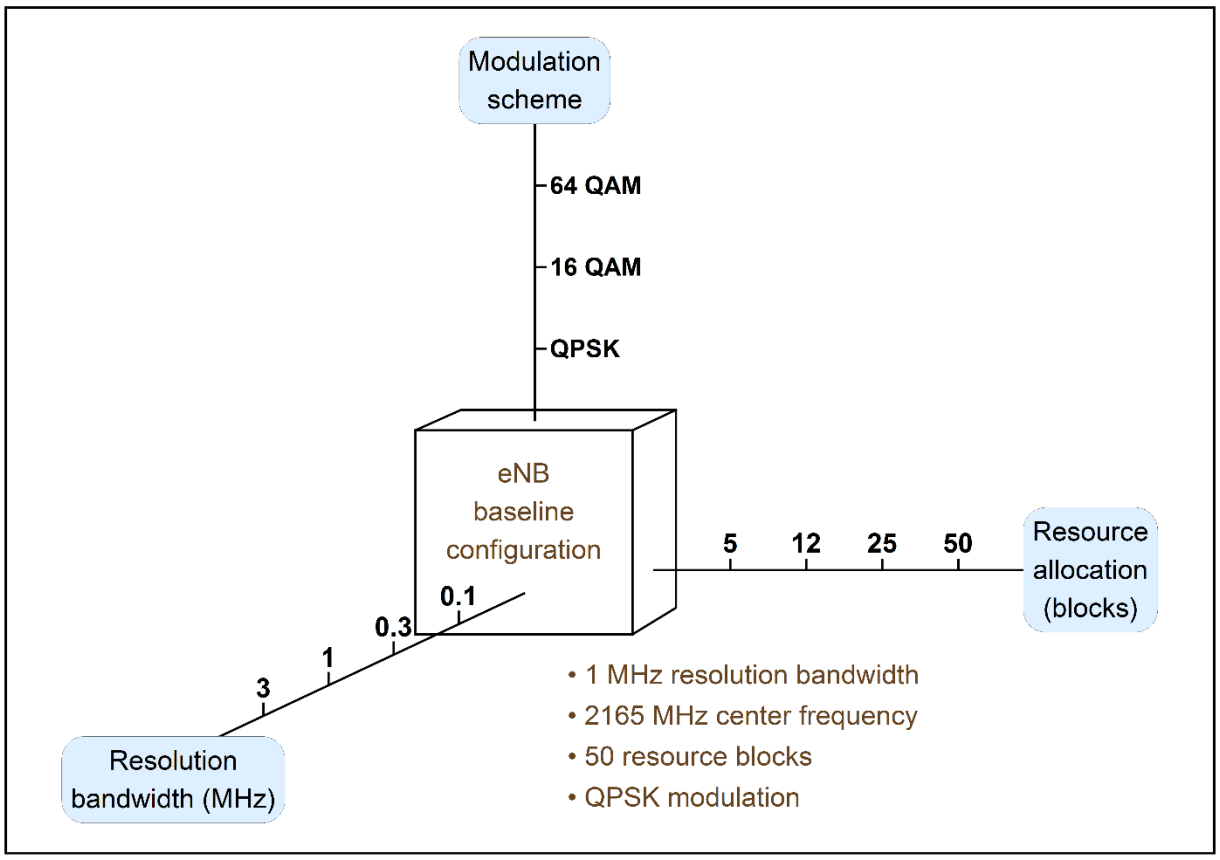

Figure 13. LTE eNB experiment plan. The eNB experiment was conducted per a one-factor-at-a-time plan that studied three factors, RBW, resource allocation, and modulation scheme.

7.2. UE Handset Experiment Plan

The UE plan addressed three experimental factors: resource allocation, UE handset model, and RBW. Resource allocation and UE handset model were both considered to potentially significantly affect OoB spectral content. RBW was again included as a study factor to assess the potential impact to different receivers. The three factors were varied one-factor-at-a-time in the experiment proceeding from a baseline handset configuration consisting of a QPSK transmission with a full 50 resource block allocation at a 1775 MHz center frequency measured with a 1 MHz resolution bandwidth. The UE handset experiment plan is shown in Figure 14.

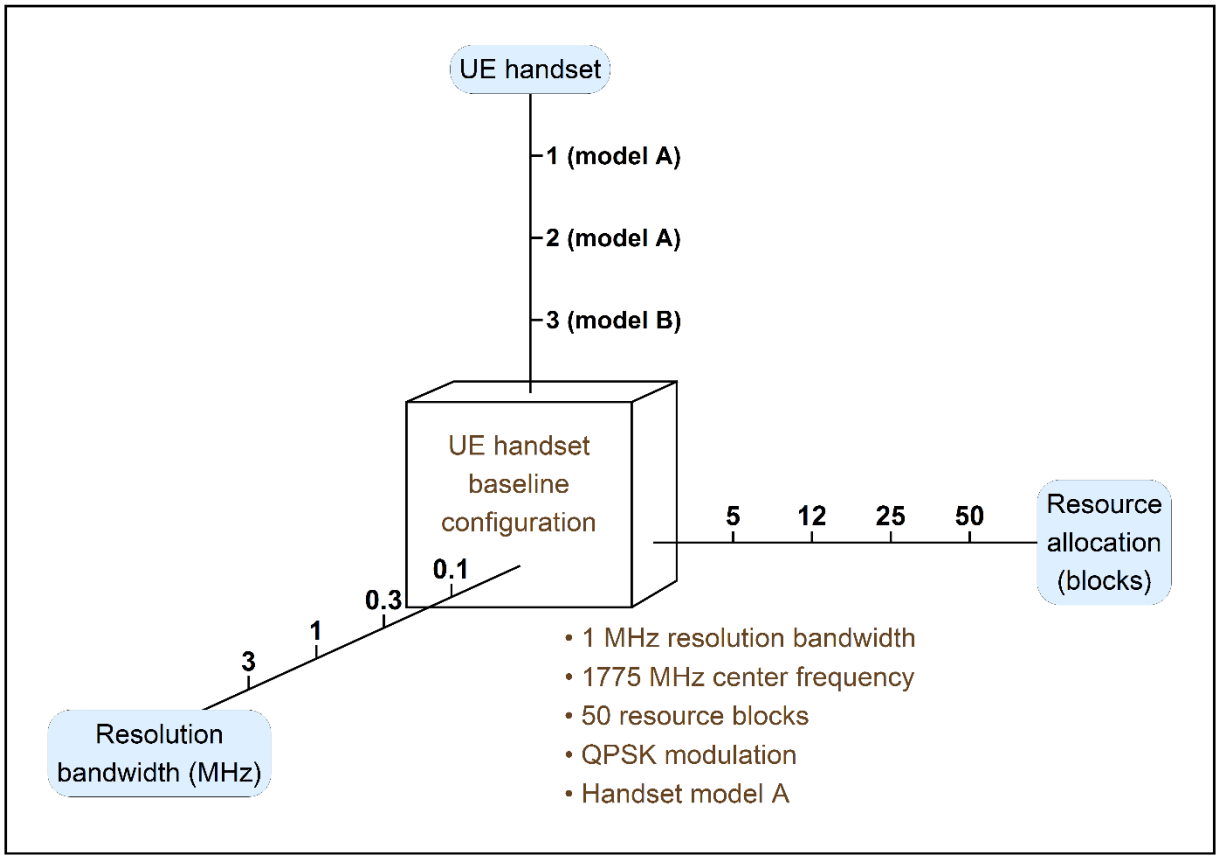

Figure 14. LTE UE handsets experiment plan. The UE handset experiment was conducted per a one-factor-at-a-time plan with three factors, resolution bandwidth, resource allocation, and handset.

8. Measurement Results and Analysis for eNB and UE data collections.

8.1. eNB Data Collection

The data collection plan to support the eNB experiment had 40 hours planned for spectral measurements (frequency scans). Each power spectrum was measured in two parts, a left scan covering the spectrum below and just above the eNB center operating frequency and a right scan covering above and just below the center frequency. The data collection plan called for a sequence of four replicate measurement blocks, each block consisting of a set of left scans followed by a corresponding set of right scans, as shown in Figure 15.

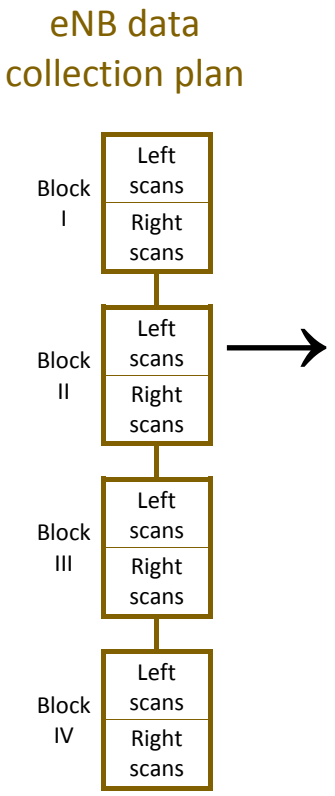

Detail – Block II left scans

Scan	Type	Resolution bandwidth (MHz)	Resource allocation (blocks)	Modulation scheme
1	Calibration			
2	Calibration			
3	eNode B	1	50	QPSK
4	eNode B	3	50	QPSK
5	eNode B	0.3	50	QPSK
6	eNode B	0.1	50	QPSK
7	Calibration			
8	Calibration			
9	Calibration			
10	Calibration			
11	eNode B	1	25	QPSK
12	eNode B	1	12	QPSK
13	eNode B	1	5	QPSK
14	eNode B	1	50	16QAM
15	eNode B	1	50	64QAM
16	Calibration			
17	Calibration			

Figure 15. eNB data collection plan. The plan is comprised of four replicate blocks executed in sequence. Each block is comprised of a set of left scans followed by a set of right scans. The detail at right shows, for example, the 17 scans made in Block II. The shaded scan in the detail is the experiment's baseline configuration. Each of the eight sets of scans (four left and four right) has the same sequence of 17 scans.

The systematic scan sequence specified in Figure 15 for the eNB data collection plan was chosen over a more robust randomized scan sequence to minimize laboratory operator error and because of the relatively small number of scans involved in the plan.

8.2. eNB Results

The results of the eNB experiment are summarized in a series of plots (Figures 16– 19). All plots show both RMS and peak power spectra, with both spectra plotted relative to 0 dB maximum

observed RMS power. While data were collected over broader frequency ranges, the spectral plots were limited to the frequency range 2060–2210 MHz so that details of the spectra could be examined. No eNB transmitter signal was observed above the noise floor outside 2060–2210 MHz in any of the collected data.

The chosen eNB operating center frequency was 2165 MHz for the presented eNB spectral measurements. The spectra in each plot are made up of data from two frequency scans: a left scan from lower frequencies to beyond 2165 MHz and a right scan below 2165 MHz and scanning to higher frequencies. This accounts for the small discontinuities present in the plotted spectra at the 2165 MHz center frequency.

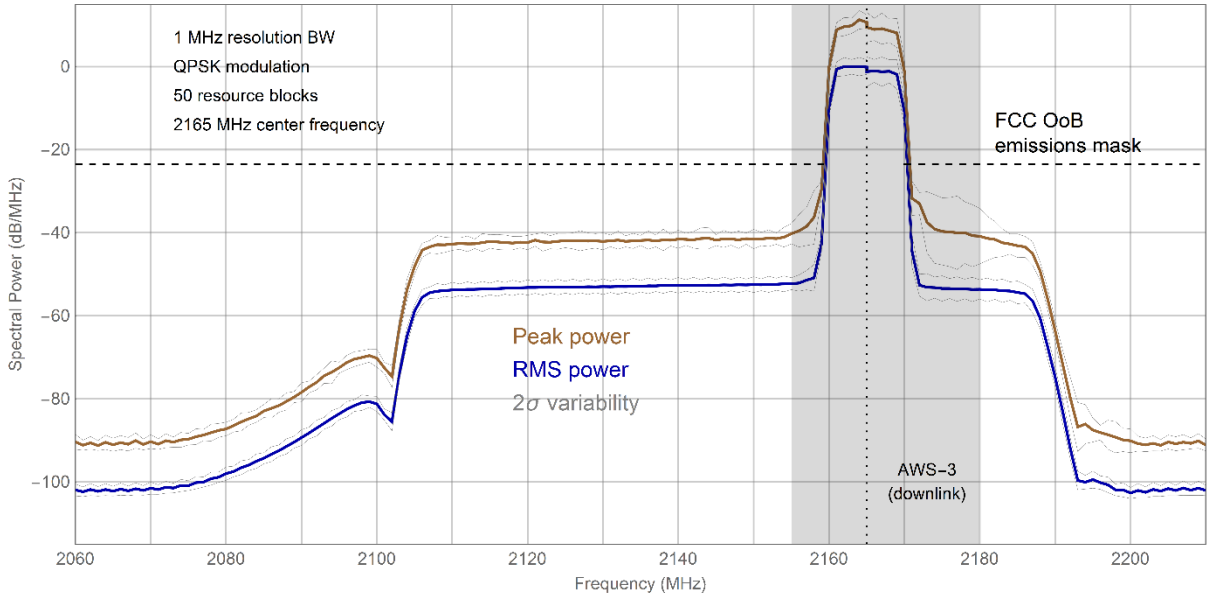

Figure 16. LTE eNB power spectrum with its baseline configuration. The RMS and peak power spectra are enveloped by curves at plus/minus two standard deviations (2σ) to indicate the spectral variability. The average 2σ variability in the RMS and peak power spectra across the presented frequency range are ±1.8 dB and ±2.4 dB, respectively.

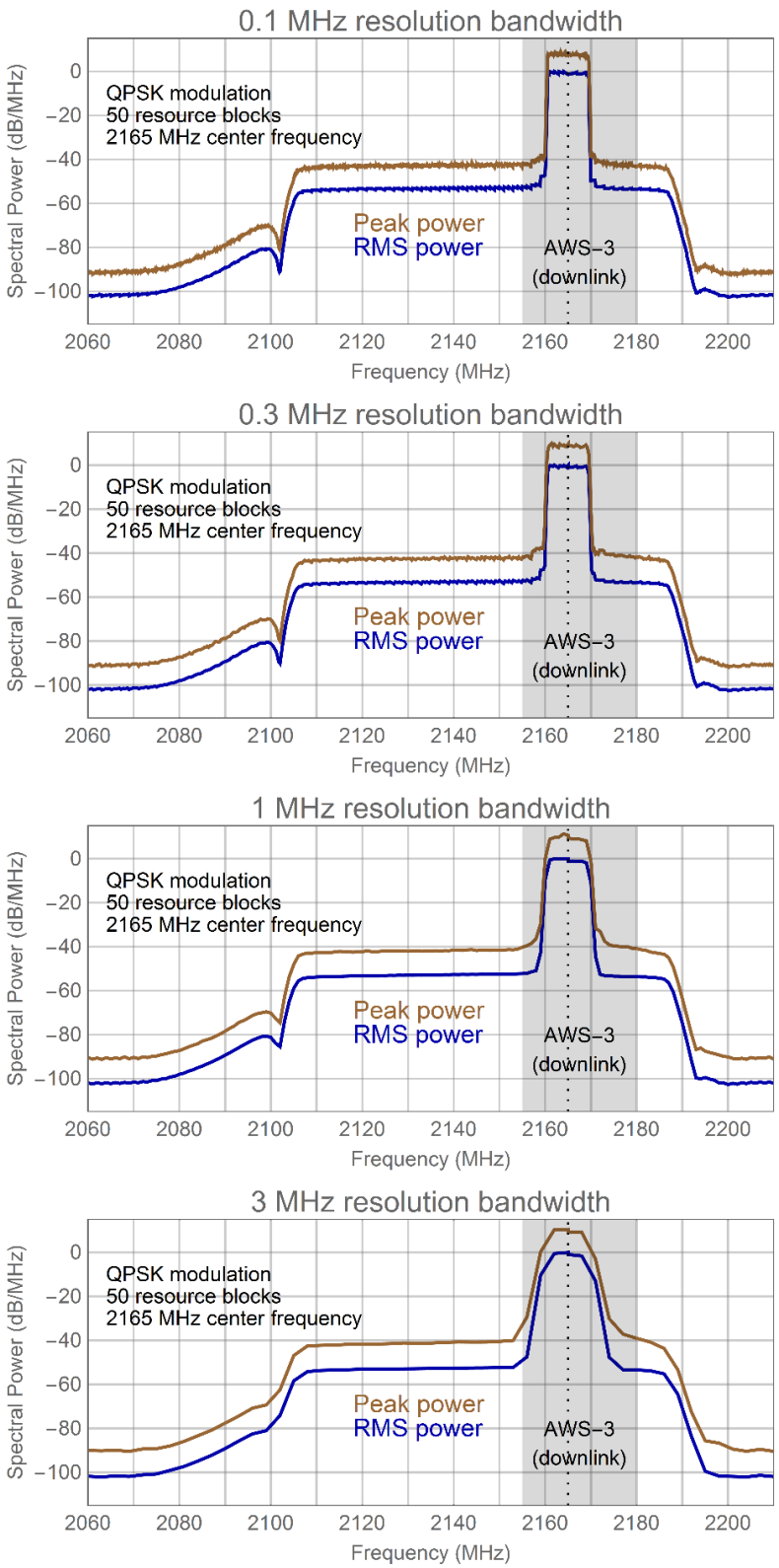

Figure 17. LTE eNB in its baseline configuration at four different resolution bandwidths (100 kHz, 300 kHz, 1 MHz, and 3 MHz).

The eNB RMS and peak power spectra varied depending on the resource allocation. Figure 18 shows that the peak power spectrum was nearly the same for 5, 12, 25, and 50 resource blocks across the plotted 2165–2205 MHz frequency range, except near 2175 MHz where there was some evidence for slightly increased peak power with 50 resource blocks. Predictably, though, the RMS power spectrum showed (see Figure 18 detail) increased power over a progressively broader portion of the range 2160–2170 MHz as the resource allocation increases from 5 to a full 50 blocks.

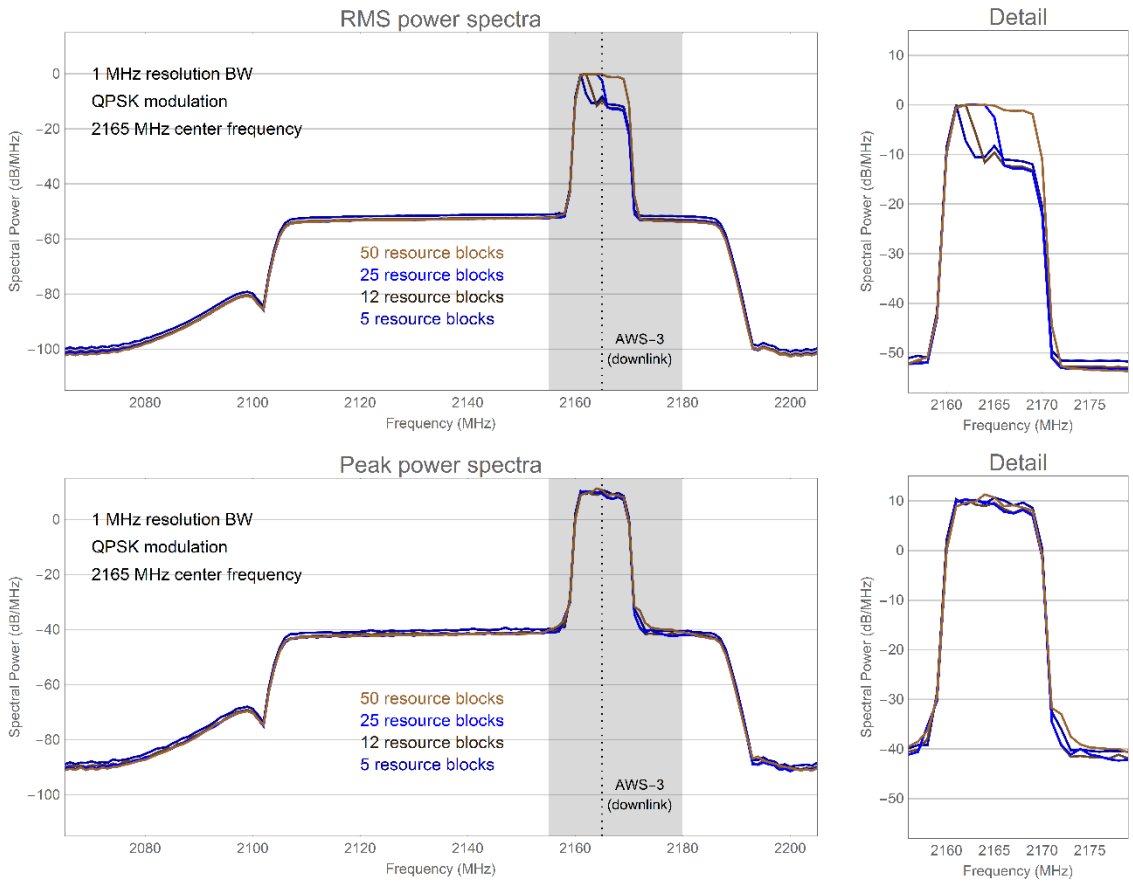

Figure 18. LTE eNB power spectra with allocations of 5, 12, 25, and 50 resource blocks. The upper plot and its detail show RMS power spectra; the lower plot and detail show peak power spectra.

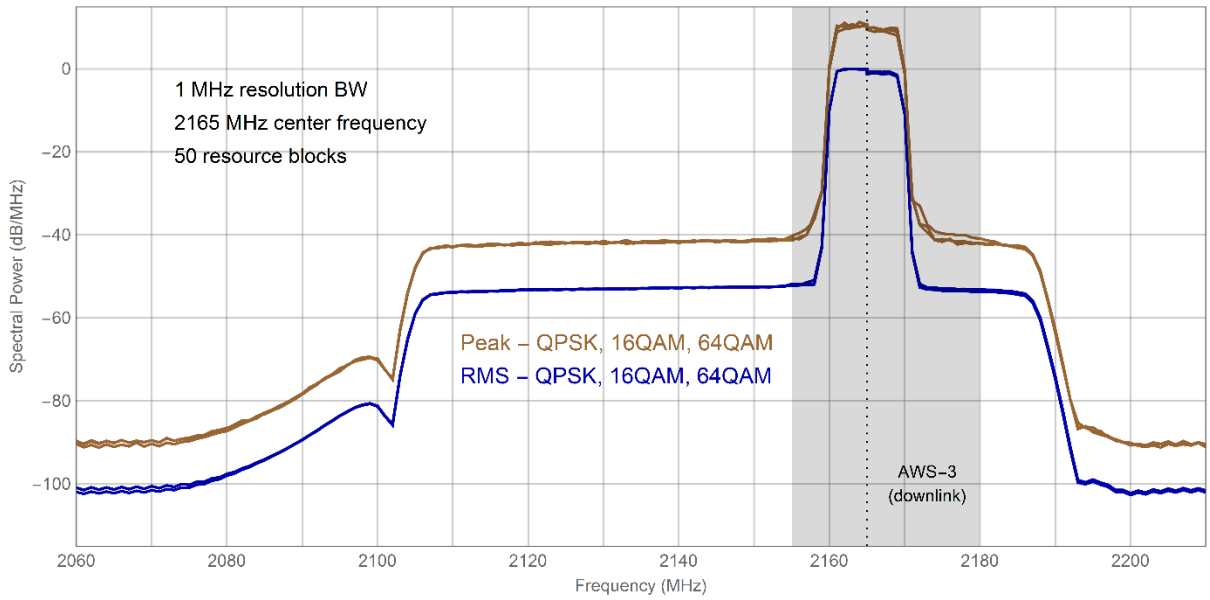

Figure 19. LTE eNB power spectra with QPSK, 16QAM, and 64QAM modulation schemes. In the eNB's baseline configuration the RMS and peak power spectra do not differ significantly due to modulation scheme.

8.3. UE Data collection

The data collection plan for the UE experiment paralleled that used in the eNB experiment. The UE plan had 40 hours planned for spectral measurements (frequency scans). Each power spectrum was measured in two parts, a left scan covering the spectrum below and just above the eNB center operating frequency and a right scan covering above and just below the center frequency. The data collection plan specified a sequence of three replicate measurement blocks, each block consisting of a set of left scans followed by a corresponding set of right scans, as shown in Figure 20.

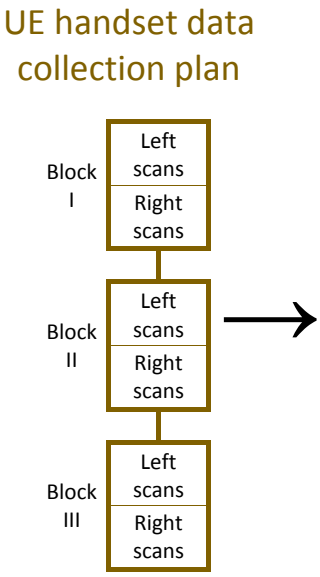

Detail – Block II left scans

Scan	Type	Resolution bandwidth (MHz)	Resource allocation (blocks)	UE handset
1	Calibration			
2	Calibration			
3	Calibration			
4	UE handset	1	50	1
5	UE handset	3	50	1
6	UE handset	0.3	50	1
7	UE handset	1	25	1
8	UE handset	1	12	1
9	UE handset	1	5	1
10	UE handset	1	50	2
11	UE handset	3	50	2
12	UE handset	0.3	50	2
13	UE handset	1	25	2
14	UE handset	1	12	2
15	UE handset	1	5	2
16	UE handset	1	50	3
17	Calibration			
18	Calibration			
19	Calibration			

Figure 20. UE handset data collection plan. The plan is comprised of three replicate blocks executed in sequence. Each block is comprised of a set of left scans followed by a set of right scans. The detail at right shows, for example, the set of 19 left scans made in Block II. The shaded scans in the detail are the experiment's baseline configuration. Each of the six sets of scans (three left and three right) has the same sequence of 19 scans.

In both the UE and the eNB experiments, DUT frequency scans were sandwiched between calibration scans. This was done so that the calibrations could be tested for drift over the time period of the device scans. Significant drift sometimes occurred (discussed in Appendix B). The calibration curve applied to each measured device scan was the average of all the calibration scans that sandwiched the DUT scan. The variability within the collection of calibrations associated with each measured device scan was accounted for in the experiments' uncertainty analyses (Appendix A).

8.4. UE Results

The results of the UE handset experiment are summarized in a series of plots (Figures 21 – 25). All plots show both RMS and peak power spectra, with both spectra plotted relative to 0 dB maximum observed RMS power. While data were collected over broader frequency ranges, the spectral plots were limited to the frequency range 1670–1820 MHz so that details of the spectra could be examined. No UE signal was observed above the noise floor outside 1670–1820 MHz.

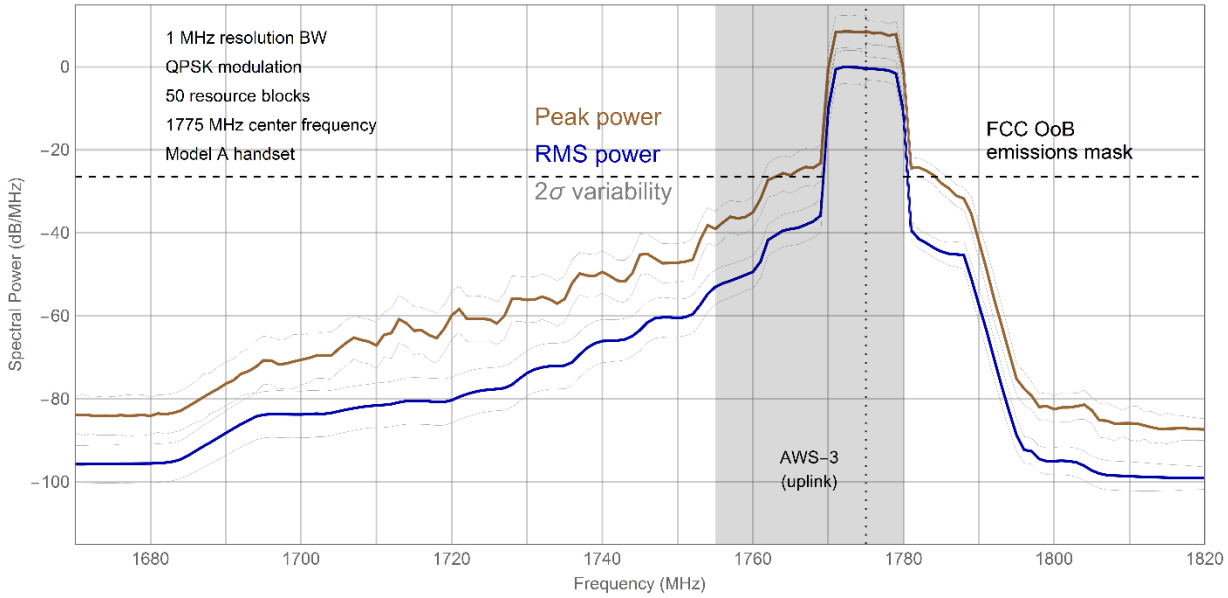

Figure 21. LTE UE handset power spectrum with its baseline configuration. The RMS and peak power spectra are enveloped by curves at plus/minus two standard deviations (2σ) to indicate the spectral variability. The spectra are averaged over the two model A handsets. The average 2σ variability in the RMS and peak power spectra across the presented frequency range are ±2.2 dB and ±2.3 dB, respectively.

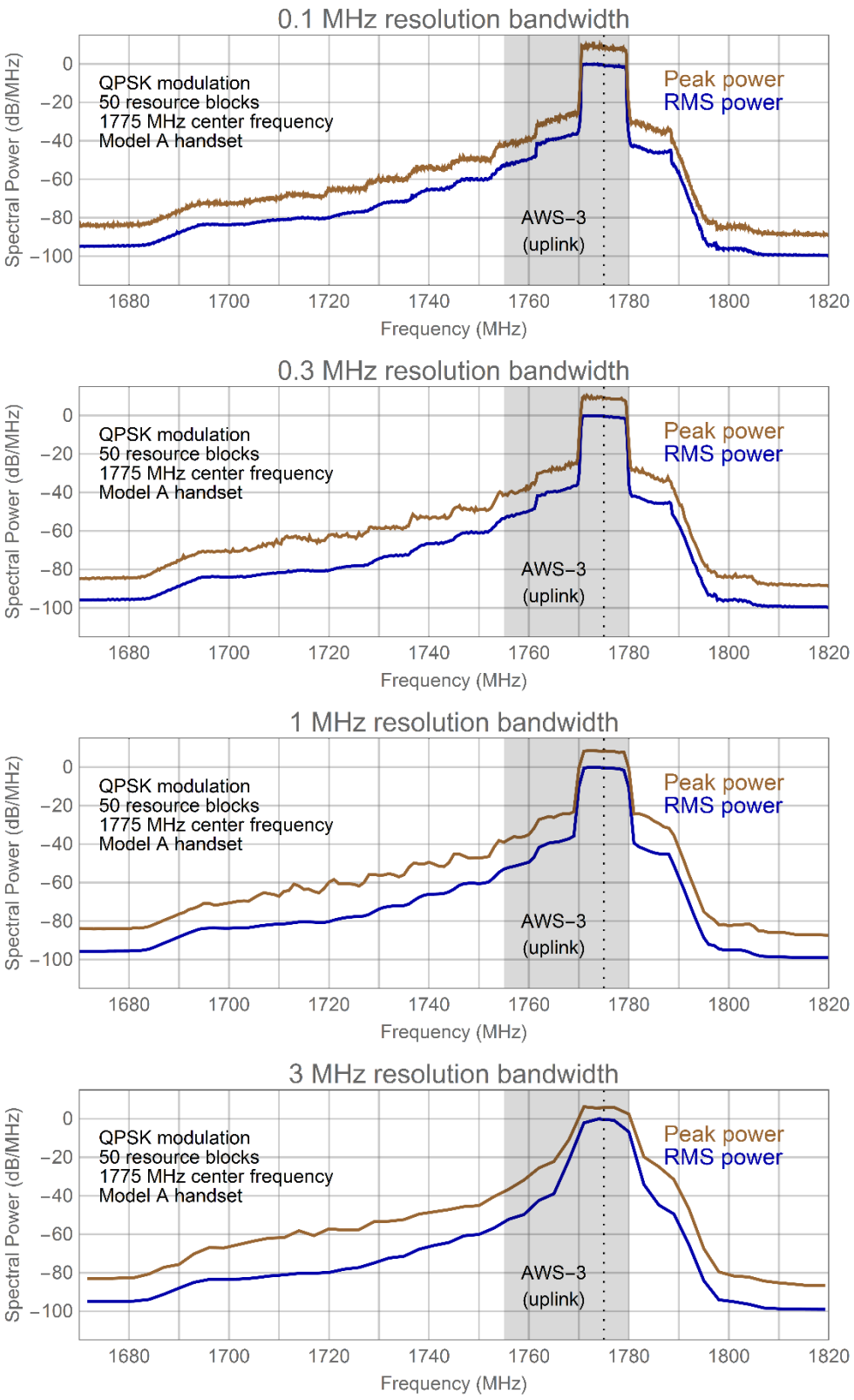

Figure 22. LTE UE handset in its baseline configuration at four different resolution bandwidths (100 kHz, 300 kHz, 1 MHz, and 3 MHz). All spectra are averages for the two model A handsets.

The UE handset RMS and peak power spectra varied similarly depending on the resource allocation. Both the RMS and peak power spectra showed (see Figure 23 details) increased power over a progressively broader portion of the 1770–1780 MHz frequency range as the resource allocation increased to a full 50 blocks. This similar variation in the UE handset RMS and peak power spectra was distinctly different from corresponding variation seen for the eNB, in which RMS power varied with resource allocation but peak power did not.

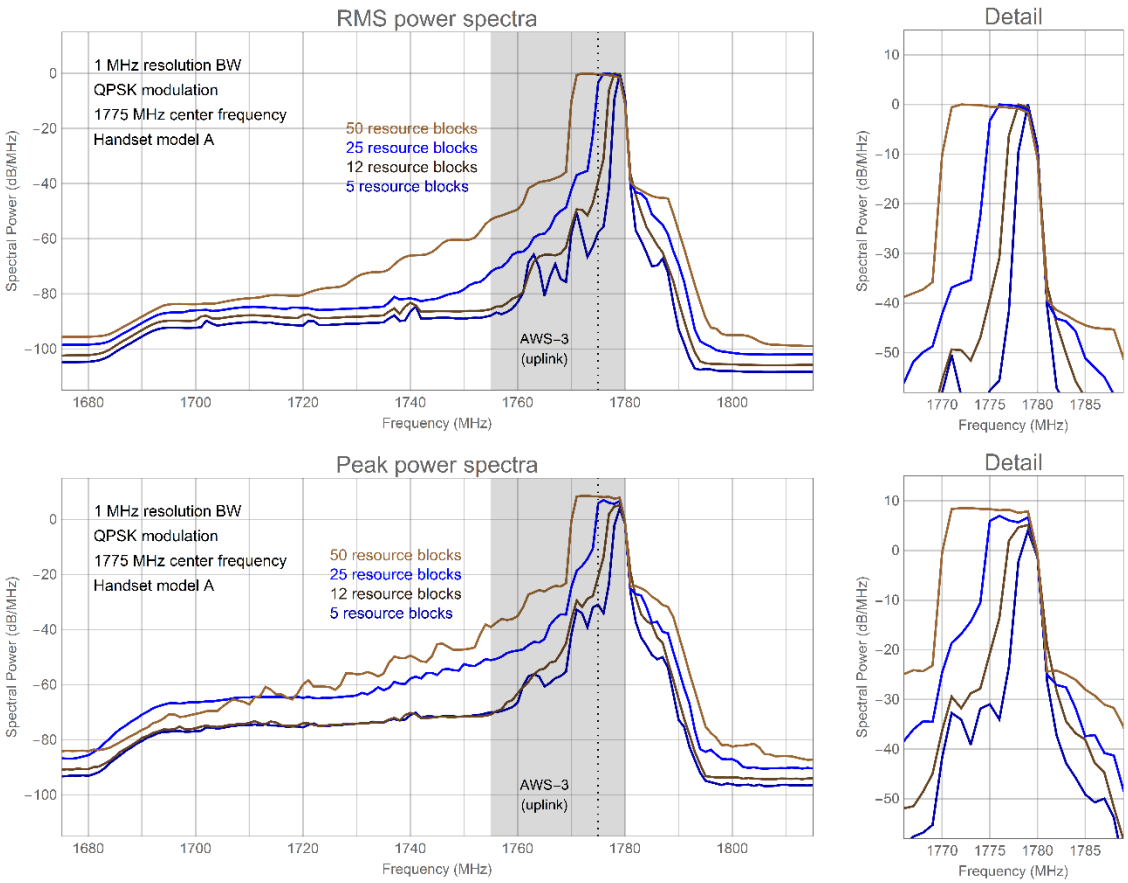

Figure 23. UE handset power spectra with allocations of 5, 12, 25, and 50 resource blocks. The upper plot and its detail show RMS power spectra; the lower plot and detail show peak power spectra.

Three different LTE UE DUTs were measured under baseline conditions. Two of the UEs were of the same model (A) while the third was of a model (B) from a different manufacturer. This constellation of UEs allowed an assessment of the spectral variation both within same model handsets and among handsets of different models. Figure 24 shows the measured RMS and peak power spectra for the three UEs. The plots show that 1) the spectra of the three UEs were similar across the full displayed 1670–1820 MHz frequency range, 2) the spectra of the two model A UEs were identical to less than 1 dB almost everywhere within the presented frequency range, and 3) the variability among the different UEs was greater than that seen for the two model A UEs. This last point was not surprising; it does, though, underscore the possibility that other UE models might exhibit spectra at some variance with those measured for models A and B.

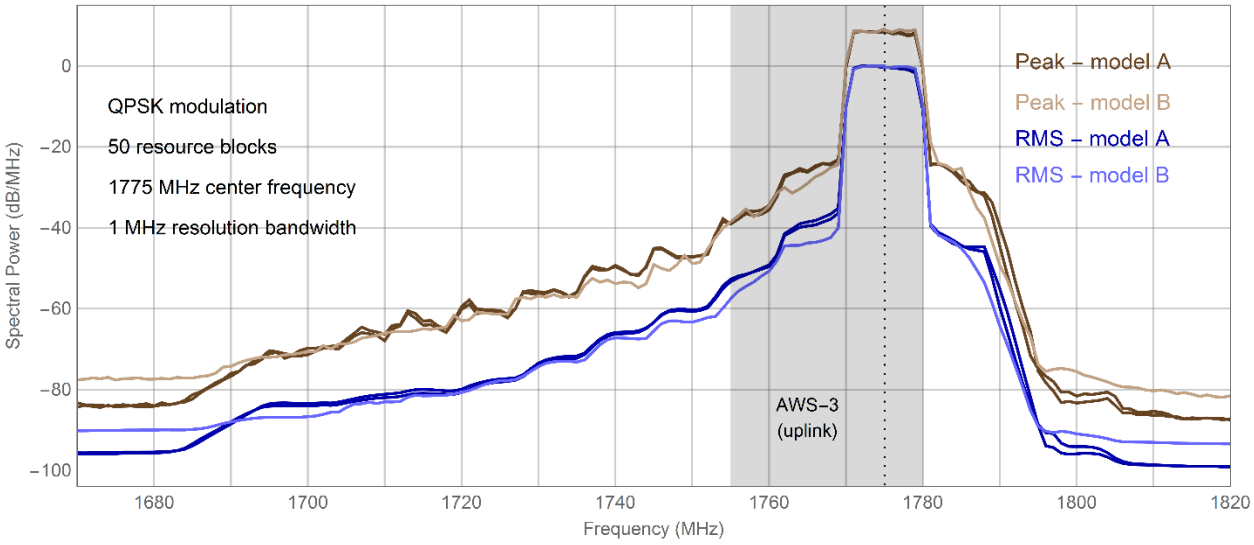

Figure 24. Power spectra of three LTE handsets, two model A and one model B. The three blue curves (darker for model A and lighter for model B) are RMS power spectra and three the brown curves (darker for model A and lighter for model B) are peak power spectra. The spectra for each handset are 0 dB referenced to that handset's maximum RMS power.

Modulation type was not a factor included in the design of the UE handset experiment. The CMW-500 emulator used in the UE experiment (Figure 6), though, can select the UE modulation scheme. To determine if modulation type should be an experiment design factor the team performed frequency scans for one of the Model A UEs under baseline conditions to compare QPSK modulation with 16QAM. The results are shown in Figure 25. The RMS power spectra of the two modulation types closely agreed in this baseline comparison; the peak power spectra disagreed in a limited way at around 1700 MHz where QPSK exhibited as much as 10 dB/MHz greater peak power density than 16QAM. No corresponding difference were observed in eNB spectra with different modulation schemes (see Figure 19).

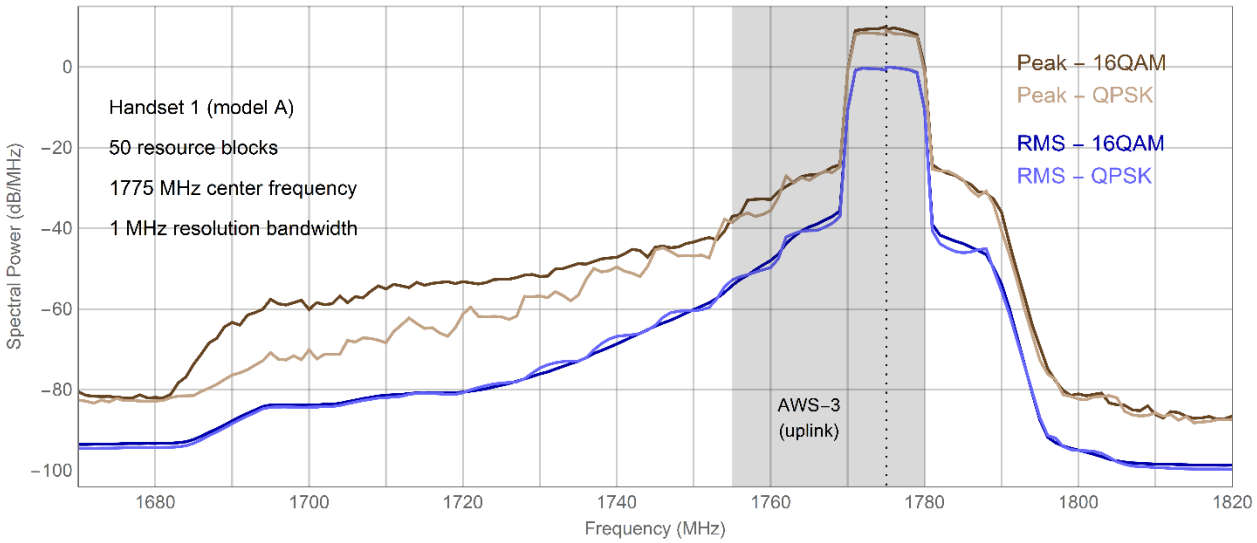

Figure 25. Baseline comparison of LTE UE handset power spectra with 16QAM and QPSK modulation schemes.

9. Summary and Conclusions

Deployed AWS-3 radio systems will abut spectral bands currently used by AMT systems at federal test and training ranges. Out-of-band and spurious emissions from AWS-3 LTE eNB base stations and UE handsets could potentially interfere with these incumbent AMT systems. Electromagnetic interference analyses to address this concern depend on knowledge of the power spectra of the AWS-3 eNBs and UE handsets in the frequencies used by (and in the receiver bandwidths of) these adjacent-band systems. The experiments in this investigation were undertaken to support such analyses.

Laboratory measurements of AWS-3 eNB and UE handset transmitter power were made using adaptive attenuation to obtain RMS average and peak power spectra with dynamic ranges exceeding 100 dB. These measured frequency scans extend 200 MHz and more, deep into the frequency bands adjacent to AWS-3 bands. Measurements were made in two separate experiments, one conducted with an eNB base station and one with three UE handsets. The two experiments used one-factor-at-a-time designs with resource allocation, resolution bandwidth, modulation scheme, and handset model as factors.

The experiments' results are presented in a series of plots (Figures 16–19, 21–25) and show, most significantly, that AWS-3 eNB and UE handset spectral densities were down by 90–100 dB (at least) in the telemetry bands adjacent to the AWS-3 bands. The two experiments further reveal that AWS-3 transmitter peak powers are about 10 dB above RMS average powers and that, while the number of resource blocks allocated for a transmission had the expected effect on in-band spectral signature, OoB emissions are insensitive to resource allocation. Similarly, AWS-3 eNB and UE OoB emissions were both found to be insensitive to modulation scheme, including QPSK, 16QAM, and 64QAM. The UE handset experiment involved three UE handsets, two handsets of one model (A) and a third of a second model (B). The results in the handsets experiment showed (Figure 24) that the power spectra of different model handsets varied considerably, and the possibility exists that other (and future) handset models may exhibit power spectra at some variance with those measured for models A and B.

Calibration and effective use of laboratory time were important considerations in each of the two experiments. Each set of measurements was "sandwiched" by multiple calibrations with a noise diode both before and after the time of the measurements. Drift in the calibration curves was sometimes observed, confirming the need for frequent calibration. Frequency scans were computer-driven with automatic attenuation adjustments to capture transmitter powers over a wide dynamic range. Computer-controlled scans allowed the frequency scans to be accomplished with the best use of laboratory time and minimal chance of operator error. Each frequency scan was made in two pieces, left and right, so that the YIG filter could be correspondingly off-tuned to address coffin-cornering and still allow frequency scans to be made under computer control. A similar combination of sandwiched calibration, automated frequency scan sequencing, and scans made in left/right segments to accommodate off-tuning is recommended for consideration for future experiments of transmitter OoB emissions.

10. References

[1] FCC Report and Order: "Amendment of the Commission's Rules with Regard to Commercial Operations in the 1695-1710 MHz, 1755-1780 MHz, and 2155-2180 MHz Bands", paragraph 62. March 31, 2014. Retrieved from https://transition.fcc.gov/Daily_Releases/Daily_Business/2014/db0401/FCC-14-31A1.pdf.

[2] Sanders, G. A., J. E. Carroll; F. H. Sanders; R. L. Sole and R. J. Achatz, "Emission Spectrum Measurements of a 3.5 GHz LTE Hotspot," NTIA Technical Report TR-15-512, U.S. Department. of Commerce, Feb. 2015. Retrieved from https://www.its.bldrdoc.gov/publications/2790.aspx.

[3] 3GPP TR 36.101 "Evolved Universal Terrestrial Radio Access (E-UTRA); User Equipment (UE) radio transmission and reception." Retrieved from https://portal.3gpp.org/desktopmodules/Specifications/SpecificationDetails.aspx?specificationId=2411.

[4] 3GPP TR 36.141 "Evolved Universal Terrestrial Radio Access (E-UTRA); Base Station (BS) conformance testing." Retrieved from https://portal.3gpp.org/desktopmodules/Specifications/SpecificationDetails.aspx?specificationId=2421.

[5] North American Ericsson Mobility Report, November 2015. Retrieved from http://www.ericsson.com/res/docs/2015/mobility-report/emr-nov-2015-regional-report-north-america.pdf#page=2&zoom=100,-74,446.

[6] Counterpoint Research, study results. Retrieved http://www.insidermonkey.com/blog/10-most-sold-cell-phones-in-america-in-2015-370257/.

[7] Sanders, F.H.; Hinkle R.L.; Ramsey B.J., "Measurement procedures for the radar spectrum engineering criteria (RSEC)," NTIA Technical Report TR-05-420, U.S. Department of Commerce, National Telecommunications and Information Administration, March 2005. Retrieved from http://www.its.bldrdoc.gov/publications/2450.aspx.

[8] Sanders, G.A.; Carroll, J.E.; Sanders, F.H.; Sole, R.L.; Achatz, R.J., "Emission spectrum measurements of a 3.5 GHz LTE hotspot," NTIA Technical Report TR-15-512, U.S. Department of Commerce, National Telecommunications and Information Administration, February 2015. Retrieved from http://www.its.bldrdoc.gov/publications/2790.aspx.

[9] Sanders, F.H.; Sole, R.L.; Carroll, J.E.; Secrest, G.S.; Allmon, T.L., "Analysis and Resolution of RF Interference to Radars Operating in the Band 2700-2900 MHz from Broadband Communication Transmitters," NTIA Report 13-490. Retrieved from http://www.its.bldrdoc.gov/publications/2684.aspx.

[10] Montgomery, D. C., *Design and Analysis of Experiments, 8th Edition*, Hoboken, NJ: John Wiley & Sons, Inc., 2013.

[11] Sanders, F, "Derivations of Relationships Among Field Strength, Power in Transmitter-Receiver Circuits and Radiation Hazard Limits," NTIA Technical Memorandum TM-10-469, National Telecommunications and Information Administration, U.S. Dept. of Commerce, Jun. 2010. Retrieved from https://www.its.bldrdoc.gov/publications/2507.aspx.

Acknowledgment

The scientific and logistical support of Keith Hartley and Mark Lofquist of MITRE Corporation are gratefully acknowledged.

Appendix A Uncertainty Analysis Discussion

This appendix describes the methods used to compute the uncertainties reported for power spectra in the eNB and UE handset experiments. All computations are based in dB units unless otherwise stated. The described methods are applied individually to each frequency in the scanned power spectra of each device.

A.1. Estimated Power and Associated Uncertainties

The spectral powers directly recorded at each frequency in a scan in the eNB and UE handset experiments are uncalibrated. They are also uncorrected for the different attenuations introduced to manage the dynamic range of the device's power. After calibration and attenuation correction, the power (in dB) at each frequency is

$$P_i = R_i + G_i + A_i, \tag{A-1}$$

where R_i represents the raw recorded power (RMS or peak), G_i is the gain correction through calibration, and A_i is the attenuation correction for the i^{th} block of measurements ($i = 1, \dots, I$). In the eNB experiment $I = 4$ blocks of measurements were made. In UE handset experiment $I = 3$ blocks of measurements were made. ($I = 4$ in the UE handset experiment in the 0.3 MHz resolution bandwidth case where an additional set of scans was made.) The power spectra reported from this study are averages

$$\bar{P} = \frac{1}{I}\sum_{i=1}^{I} P_i \tag{A-2}$$

of I measurements of calibrated, attenuation-corrected powers for each frequency; in the case of UE handset spectra, the averages are over both blocks and the two model A handsets. Peak and RMS power assume a distribution of values at each frequency depending on time (represented by block), handset, etc. The reported uncertainties

$$u(P) = \left(\frac{1}{I-1}\sum_{i=1}^{I}(P_i - \bar{P})^2\right)^{1/2} \tag{A-3}$$

are sample estimates of the standard deviation of these distributions. The uncertainty associated with the reported mean spectral power $\bar{P}$ is the standard error

$$u(\bar{P}) = \frac{u(P)}{\sqrt{I}}. \tag{A-4}$$

The distinction between epistemic uncertainty $u(\bar{P})$ in average power and the aleatoric uncertainty $u(P)$ associated with the essential variability in observed RMS power is illustrated in Figure A-1— $u(\bar{P})$ is our uncertainty about the mean power while $u(P)$ is the variability that the power evidences. $u(P)$ is the uncertainty reported in Figures 16 and 21.

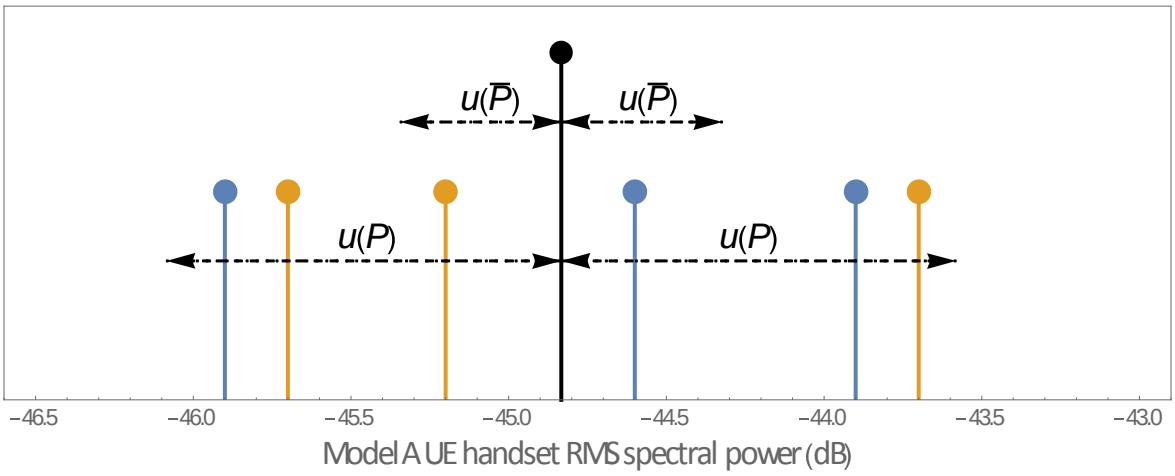

Figure A-1. Six observed RMS spectral powers of model A UE handsets at 1785 MHz under baseline conditions. Blue points are handset #1 powers; gold points are handset #2 powers; the black point is the mean of the six powers. $u(\bar{P})$ is the uncertainty in the estimate of the mean and $u(P)$ is the variability in the model A handset power.

A.2. Uncertainty of Calibration-Corrected Power

Assuming G_i, R_i, and A_i are independent, the squared uncertainty associated with P_i is

$$u^2(P_i) = u^2(G_i) + u^2(R_i) + u^2(A_i). \tag{A-5}$$

The squared uncertainty associated with R_i,

$$u^2(R_i) = \frac{\sum_{i=1}^{I}(R_i - \bar{R})^2}{I-1}, \tag{A-6}$$

is the sample variance of the I values. The uncertainty associated with G_i is discussed in section A.3. The uncertainty associated with A_i varies depending on the value of attenuation. The manufacturer's specified uncertainties are shown in Table A-1.

Table A-1. Manufacturer's specified attenuation uncertainties for a frequency range of DC to 20 GHz.

Attenuation, A_i (dB)	0	10	20	30	40	50	60	70	80
Uncertainty, $u(A_i)$ (dB)	0.12	0.16	0.16	0.17	0.32	0.36	0.36	0.52	0.50

Assuming the uncertainties for each P_i are similar across blocks, we pool the $u^2(P_i)$ using

$$u^2(P) = \frac{1}{I}\sum_{i=1}^{I} u^2(P_i)\,. \tag{A-7}$$

We report the uncertainty associated with a single measurement of power, $u(P)$, to represent the variability in the distribution of power measurements. The same procedure is used for both RMS average and peak power.

A.3. Gain Uncertainty

The measurement equation for the gain in dB from the i^{th} block of measurements at a single frequency is

$$G_i = ENR + N_p - d_i\,, \tag{A-8}$$

where

$$d_i = 10 \cdot \log\left(D_{\mathrm{on},i} - D_{\mathrm{off},i}\right). \tag{A-9}$$

ENR is the excess noise ratio, and N_p is the noise power. The values of $D_{\mathrm{on},i}$ and $D_{\mathrm{off},i}$ are powers (in linear units) when the noise diode is "on" and "off", respectively, for the i^{th} block of measurements. The squared uncertainty of gain G_i is

$$u^2(G_i) = u^2(d_i) + u^2(ENR) + u^2\left(N_p\right), \tag{A-10}$$

assuming the quantities d_i, ENR, and N_p are uncorrelated. The standard uncertainty for ENR is 0.18 dB based on manufacturer's specifications. The uncertainty of d_i is computed from a variance component analysis based on repeated calibrations in different blocks of measurements, as discussed below.

The measurement equation for noise power, N_p, is

$$N_p = 10 \cdot \log(1000 \cdot kT) + 10 \cdot \log(B) \tag{A-11}$$

where k is Boltzmann's constant (1.38064852e-23 W·s/K), T is the ambient temperature (290 K), and B is the bandwidth in Hz. Given resolution bandwidth in MHz, we use $B = RBW \cdot 10^6$ Hz, and the noise power is

$$N_p = 10 \cdot \log(1000 \cdot kT) + 10 \cdot \log(RBW \cdot 10^6) \tag{A-12}$$

where $10 \cdot \log(RBW \cdot 10^6) = RBW_{dB}$ is the resolution bandwidth in dB. The uncertainty $u\left(N_p\right)$ of the noise power N_p is given by

$$u^2\left(N_p\right) = u^2(RBW_{dB}). \tag{A-13}$$

We have $u(RBW_{dB}) = 0.065$ dB for $RBW = 1.0$ MHz, based on the manufacturer's specified accuracy. We conservatively assume that the reported "accuracies" are standard uncertainties. We assume k and T are constants that are known without error.

A.4. Uncertainties for d_i

We estimate the uncertainties in the differences d_i using random effects models, one model for the eNB experiment and a second similar model for the UE handset experiment. For the eNB experiment the uncertainty of d_i at each frequency is obtained from the nested random-effects model [10],

$$d_{ijkl} = \mu + B_i + S_{j(i)} + G_{k(ij)} + C_{l(ijk)}, \tag{A-14}$$

where

B_i represents the i^{th} block, where $i = 1, \ldots, 4$ and B_i has mean=0 and variance=σ_B^2,

$S_{j(i)}$ represents the j^{th} set of measurements within the i^{th} block, where $j = 1, \ldots, 2$ and $S_{j(i)}$ has mean=0 and variance=σ_S^2,

$G_{k(ij)}$ represents the k^{th} group of calibrations within the j^{th} set of measurements within the i^{th} block, where $k = 1, 2$ and $G_{k(ij)}$ has mean=0 and variance=σ_G^2, and

$C_{l(ijk)}$ represents the l^{th} repeat calibration within the k^{th} group within the j^{th} set of measurements within the i^{th} block, where $l = 1, 2$ and $C_{l(ijk)}$ has mean=0 and variance= σ_C^2.

Figure 15 in section 8.1 visually describes the data structure identifying the variables in the random effects model. The right side in Figure 15 displays a block of measurements containing 17 left scans. The blocks are divided into two sets of measurements; scans 1-8 comprise one set of measurements, and scans 9-17 comprise a second set of measurements. Scans 1 and 2 are defined as a group of calibrations within the first set of measurements, and scans 7 and 8 represent a second group of calibrations sandwiching the first set of measurements. The data structure for the Block IV measurements is slightly different; it is missing calibration scans 7–10.

For a fixed measurement set, j, d_i is defined as,

$$d_i = \frac{1}{2 \cdot 2} \sum_{k=1}^{2} \sum_{l=1}^{2} d_{ijkl}\ , \tag{A-15}$$

the average of the observed d_{ijkl} values for the i^{th} block and a given set of measurements within the block. For each frequency, the analysis of variance provides estimates of the variance components. We use the squared uncertainty of a single value of d_{ijkl} to represent the uncertainty of d_i,

$$u^2(d_i) = \hat{\sigma}_B^2 + \hat{\sigma}_S^2 + \hat{\sigma}_G^2 + \hat{\sigma}_C^2\ . \tag{A-16}$$

Again, the uncertainty of a single value corresponds to the distribution of possible d_{ijkl} values.

For the UE handset experiment, the uncertainty of d_i at each frequency is obtained from the nested random-effects model,

$$d_{ijk} = \mu + B_i + G_{j(i)} + C_{k(ij)}, \quad \text{(A-17)}$$

where

B_i represents the i^{th} block of measurements, where $i = 1, \ldots, I$ and B_i has mean=0 and variance = σ_B^2,

$G_{j(i)}$ represents the j^{th} group of calibrations within the i^{th} block of measurements, where $j = 1, 2$ and $G_{j(i)}$ has mean=0 and variance = σ_G^2, and

$C_{k(ij)}$ represents the k^{th} repeat calibration within the j^{th} set of calibrations and i^{th} block of measurements, where $k = 1, \ldots, 3$ and $C_{k(ij)}$ has mean = 0 and variance = σ_C^2.

The data structure for the UE handsets differs from the eNB data structure in that there is only one set of measurements within a block.

Figure 20 in section A.3 visually represents the UE handset data structure.

For UE handset data, the blocks do not necessarily have two groups of calibrations (one group before and one group after the measurements of different configurations), so the data are unbalanced. The value of $D_{\text{on},i}$,

$$d_i = \frac{1}{2 \cdot 3} \sum_{j=1}^{2} \sum_{k=1}^{3} d_{ijk}\,, \quad \text{(A-18)}$$

is the average of the observed d_{ijk} values within a block of measurements.

For each frequency, the analysis of variance provides estimates of the variance components. We use the squared uncertainty of a single value of d_{ijk} to represent the uncertainty of $D_{\text{on},i}$,

$$u^2(d_i) = \hat{\sigma}_B^2 + \hat{\sigma}_G^2 + \hat{\sigma}_C^2\,. \quad \text{(A-19)}$$

A.5. Uncertainty Example

The three preceding sections discuss the different sources of uncertainty that combine to produce the 2σ uncertainties accompanying the eNB and UE handset spectra presented in Figures 16 and 21. These different uncertainty sources are summarized in Table A-2, each given with its associated uncertainty evaluation type (A or B). Type A uncertainty evaluations correspond to estimates from measured data, while Type B evaluations are drawn from other sources, such as manufacturer's specifications. Also shown in Table A-2 are example numerical values for each source uncertainty and for the corresponding combined standard and 2σ uncertainties, for the baseline system configuration for UE model A at the center frequency, 1775 MHz. The example illustrates the calculations that were performed at each frequency.

Table A-2. Example spectral uncertainty calculation for UE model A at the baseline system configuration with center frequency 1775 MHz (right-tuned YIG filter). Attenuation is 70 dB for this example.

Source	**Type**	**Standard Uncertainty (dB)**
$\boldsymbol{u(A_i)}$	B	0.52
$\boldsymbol{u(R_i)}$	A	1.19
$\boldsymbol{u(G_i)}$		0.78
$\boldsymbol{u(ENR)}$	B	0.18
$\boldsymbol{u(N_P)}$	B	0.07
$\boldsymbol{u(d_i)}$	A	0.76
Combined Standard Uncertainty		1.52
Expanded (2σ) Uncertainty		3.04

Appendix B Calibration

Each DUT power spectrum frequency scan in the eNB and UE handset experiments was accompanied by multiple calibration scans made both before and after the DUT scan. These calibration scans were averaged for each DUT scan to produce a calibration curve for that scan. The multiple calibration scans for each DUT scan were used to assess the variability associated with each calibration scan for a given time (before or after the device scan) and the drift in calibration over time (from before to after). Figures B-1 and B-2 show two example sets of calibration curves from the eNB and UE handset experiments demonstrating that 1) calibration scans made one immediately after another were typically highly consistent, but 2) calibration scans compared before and after a device scan sometimes differed significantly.

The eNB calibration curves in Figure B-2 are smoothed (moving average of successive pairs of power measurements) so that their differences can be visually compared more easily. In fact, the smoothing used in Figure B-2 removes a small additive zig-zag artifact present in every calibration curve in the eNB experiment. Figure B-3 shows, for example, an unsmoothed calibration curve from the eNB experiment along with its smoothed counterpart. The raw, uncalibrated eNB measurement scans all evidenced the same zig-zag artifact with the same phase and period as the calibration scans. Only unsmoothed calibration curves were used to calibrate eNB measurements. Consequently, the zig-zag artifact was effectively cancelled by the calibration procedure and the artifact did not compromise the calibrated spectral power densities obtained for the eNB.

The zig-zag artifact present in all the eNB calibration and measurement data appears in none of the data from the UE handset experiment. One potentially important difference in the two experiments is that the UE handset experiment used an external diode for calibration while the eNB experiment used a calibration diode internal to the measurement system. The two experiments were done at different physical locations in different laboratories, and poor electrical grounding may explain the zig-zag artifact in the eNB experiment.

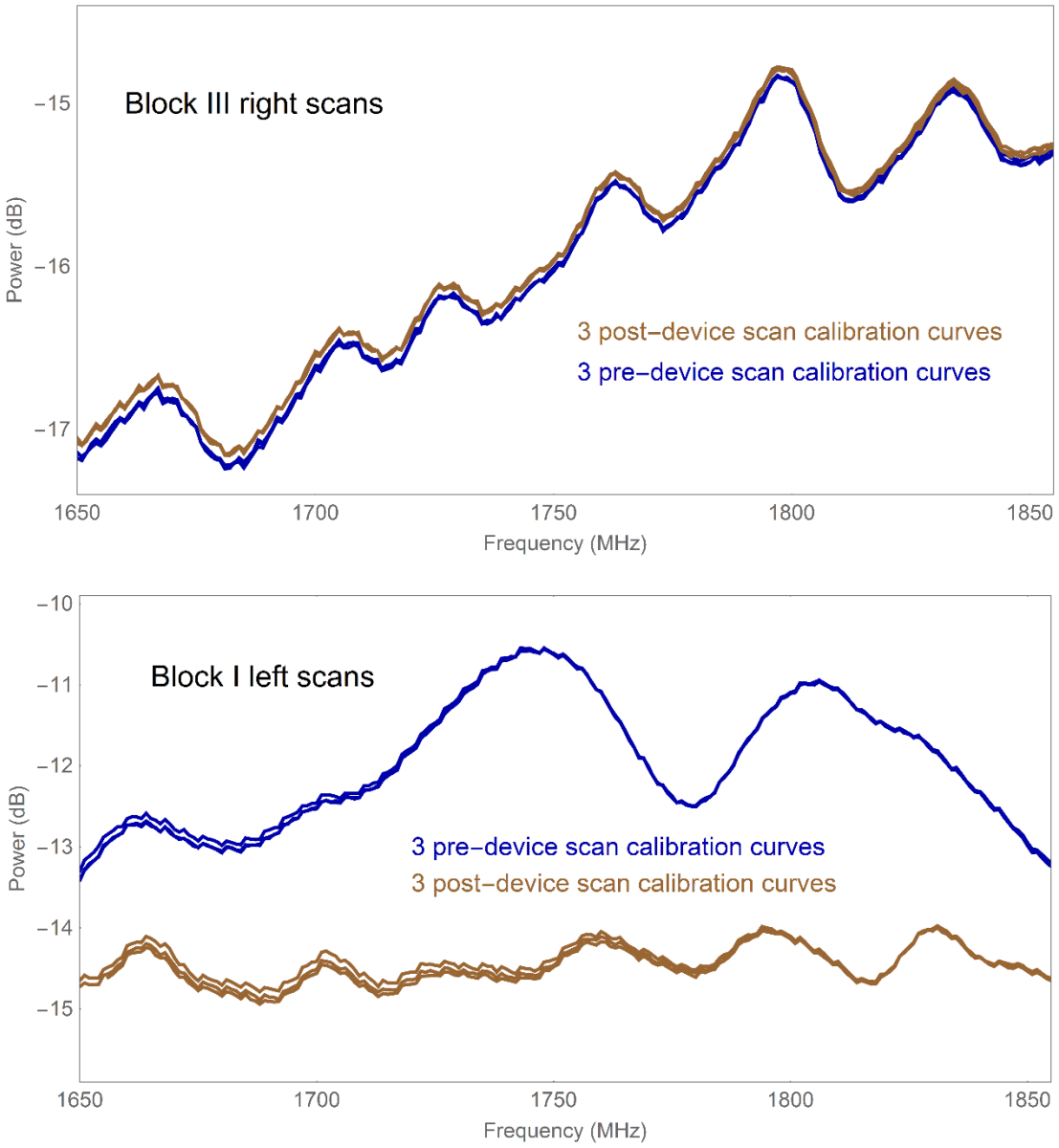

Figure B-1. Two example sets of replicate UE handset calibration curves. The top display shows the six calibration curves for Block III right scans of the UE handsets. The three calibration curves in the top display (in blue) made before the handset right scan agree well with the “after” pair (in brown). The bottom display shows the six calibration curves for Block I left scans of the handsets. The three “before” calibration curves (in blue) in the bottom display differ at some frequencies by more than 3 dB from the “after” curves. In both examples calibration scans made one immediately after another—within each group of three—are highly consistent.

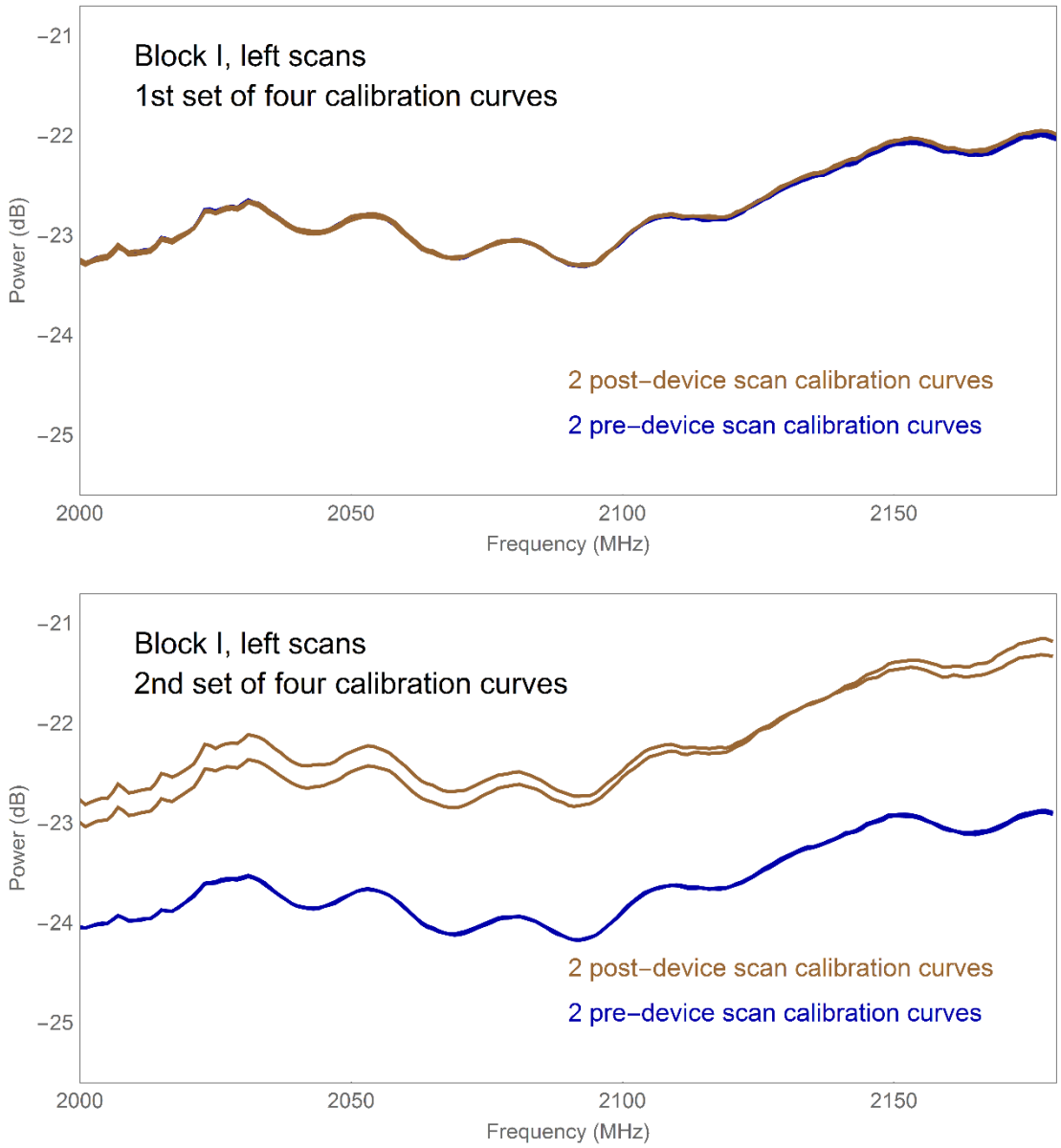

Figure B-2. Two example sets of smoothed replicate eNB calibration curves. The calibration curves are smoothed here so that they can be better compared. The two example sets of calibration curves are those called for by the eNB data collection plan for the left scans in Block 1. The top display shows the first set. The two calibration curves there (in blue) made before the eNB left scans agree well with the "after" pair (in brown). The bottom display shows the second set of calibration curves for the left scans in Block 1. The two "before" calibration curves (in blue) in the bottom display differ at some frequencies by more than 1 dB from the "after" curves. In both examples calibration scans made one immediately after another show good consistency.

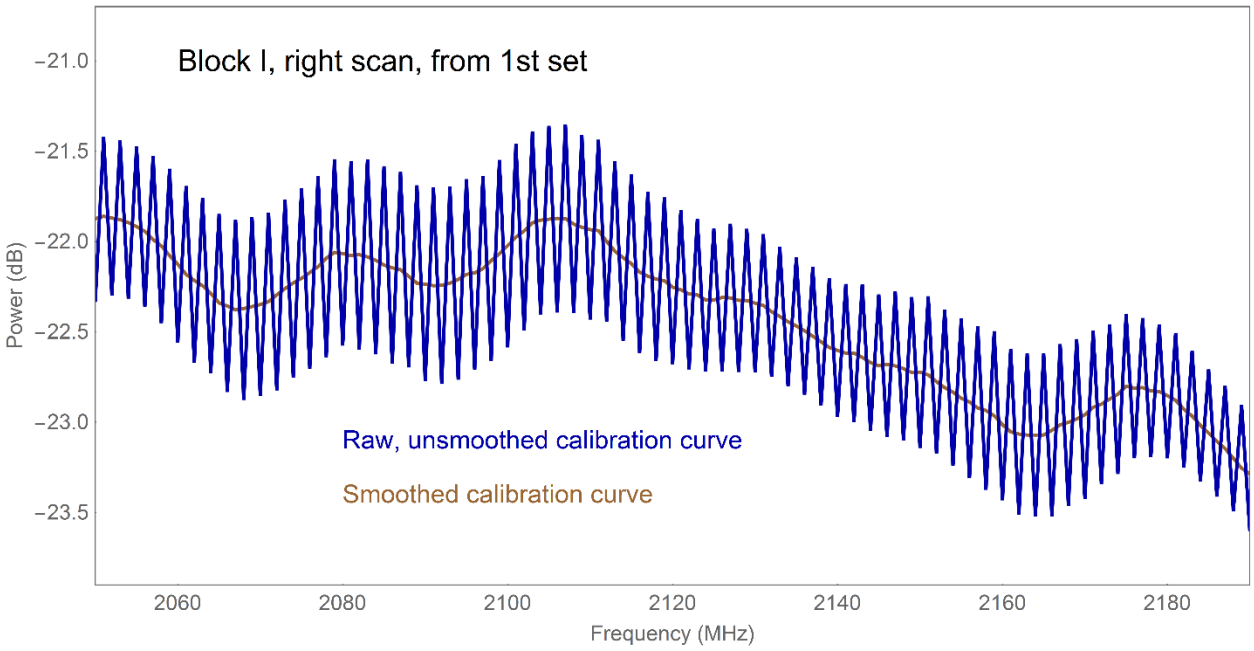

Figure B-3. An example raw, untreated eNB calibration curve and its smoothed counterpart. Smoothing was accomplished by a moving average of successive pairs of power measurements. The peak-to-peak amplitude of the zig-zag artifact in this example is as much as 1 dB at some frequencies.

Appendix C Plotting Absolute Emission Mask Limits on Relative-Power Spectra

The FCC defines limits on OoB and spurious spectrum emissions in terms of absolute spectrum power density produced in a transmitter's circuitry at the input to the transmitter's antenna. That is, it is a limit on the amount of power within a defined unit of bandwidth. An example would be some number, x, of milliwatts in a bandwidth of a megahertz. If we write x milliwatts (linear units) in decibel terms as 10log(x) = X decibels relative to a milliwatt (dBm), then the spectrum emission mask limit is written as X dBm/MHz.

C.1. Characteristics of Absolute Power Density Emission Masks

There are some things worth noting about this kind of emission limit. First, it is not a field strength limit, which would have to be defined at a point in space *outside* a transmitter. It is a limit on OoB and spurious power *within* a transmitter's circuitry. Second, it is not a total power limit; it is a power density limit (a limit on power per unit bandwidth). Third, it is independent of the total power produced by a transmitter or radiated into space on the transmitter's tuned (intentional) emission frequency or frequencies (f_0). In principle, the OoB and spurious power density of a transmitter can be measured and compared to such a mask limit without even knowing or measuring the transmitter's power at its own f_0.[13] Fourth, while a direct comparison of a transmitter's OoB or spurious emissions to such a mask limit cannot be performed using radiated emissions, indirect methods for such comparisons do exist.

This last point is worth considering in light of the fact that some transmitters cannot have their spectrum emissions measured via hardline connections to their power output ports. This is because some transmitters simply do not have such ports physically available, or may have multiple such ports. Or they may use distributed antenna arrays that lack single-point transmitter power distribution points accessible by test and measurement engineers, etc.

C.2. Relative-Power Emission Spectra Collected for EMC Studies

A further complicating factor is that EMC measurements of transmitter OoB and spurious emissions are often most usefully referenced to the maximum (either peak detected or average detected) power radiated at f_0, this power level being defined to be zero decibels relative to the rest of the spectrum. In other words, EMC spectrum measurements may most usefully be referenced as decibels relative to power measured in a bandwidth at f_0. This is because absolute transmitter power levels may not be fixed for many types of radio systems; they may instead vary as a function of, for example, multiple transmitter modes for short range versus long range communications or, for another example, narrow bandwidths for lower data rates versus wider bandwidths for higher data rates, and so forth.

With relative-level emission spectra in hand, subsequent EMC analyses progress with absolute transmitter power levels added (as it were) to the zero decibel power levels at f_0 to obtain

[13] Although, as we shall see, as a practical matter a transmitter's total mean power does need to be somehow known or established for cases in which the transmitter's OoB and spurious emissions must be radiatively measured.

compatibility results on a mode-by-mode analysis of transmitter operations, with the same additions being made to the corresponding OoB and spurious emission levels.

The data in this report were gathered for use in subsequent EMC studies and therefore are reported as relative-power spectra with power at f_0 defined as zero decibels in any given measurement bandwidth. This raises the question of how to plot absolute power density FCC emission mask limits on relative power (i.e., power in a bandwidth at f_0 equals zero decibels relative to the rest of the spectrum) data plots.

C.3. Methods for Plotting Absolute Power Emission Masks on Relative Power Emission Spectra

In this appendix, we present two methods. Both methods can be applied to the problem of plotting absolute power density mask limits on hardline-coupled measured emission spectra. But only one of the methods can be applied to radiated emission measurements, as we shall see.

In both cases, we emphasize that emission mask limits can be graphed straightforwardly only on data that were collected in the defined bandwidth of the mask's power density, i.e., if the limit is defined in 1 MHz then the mask limits should only be graphed on data that were collected in a 1 MHz measurement (effectively the same as the resolution) bandwidth. Doing this eliminates the problem of adjusting results or mask limits for data collected in other bandwidths.[14] Accordingly, in this study only data measured in a 1 MHz bandwidth were considered to be candidates for having the FCC emission mask limit graphed against them.

C.3.1. First Method for Plotting Absolute Masks on Hardline-Connected Relative Emission Spectra

The (arguably) simpler problem to solve is the graphing of the absolute power density mask limit on relative spectrum emissions that have been measured via a hardline connection to a transmitter. In this case, if the connection to the transmitter was made at the antenna port, then all of the power produced by the transmitter is contained in the connection between the transmitter and the measurement system; the measurement comports with the definition of the mask limit. This was the case for the eNB emission measurements in this study.

The problem is tractable in this case because the eNB measurements, although presented in this report in relative-power plots, were in fact measured in absolute power in the measurement system circuitry. When the in-circuit power was measured in the 1 MHz reference bandwidth, the absolute measured power levels can be compared directly the OoB and spurious emission mask limits. The comparison is done as follows.

[14] It is possible to compute correction factors to convert power measured in one bandwidth, and with a given type of detection, into the power that would have been measured in another bandwidth for any given modulation type of radio signal. The problem is tractably deterministic. But the conversion requires attention to the bandwidth dependence of the measured power. This dependence in turn depends on the type of measurement detection and the measured signal's modulation. Such bandwidth conversion analysis, although possible, is beyond the scope of the work that was to be performed for this project's sponsor.

First, we examine the expression for the mask limit itself. The suppression, *S*, of OoB and spurious emission power relative to total mean power at the fundamental frequency is defined to be

$$S = 43 + 10log(p_{transmit}) \quad \text{(C-1)}$$

where

S = suppression of the mask level relative to the total mean transmitted power (dB),

$P_{transmit}$ = total mean transmitted power (watts), and

43 = constant factor of decibels relative to a watt in 1 MHz (dBW/MHz).

If we write transmitter power in decibel units, $P_{transmit}$, where $P_{transmit} = 10\log(p_{transmit})$, then the suppression equation is

$$S = 43 + P_{transmit}. \quad \text{(C-2)}$$

Since the suppression, *S*, is calculated relative to the total mean power produced by the transmitter, the mask limit, *L*, is calculated by adding the suppression to the transmitter power

$$L = P - S = P_{transmit} - 43 - P_{transmit} = -43\frac{dBW}{MHz} = -13\frac{dBm}{MHz}. \quad \text{(C-3)}$$

On our data graphs for hardline coupled power at the eNB transmitter's antenna output port, we do not have the OoB and spurious power levels graphed in absolute terms. Instead, we have those power levels graphed relative to the output power that we measured in a 1 MHz bandwidth; the output power measured in 1 MHz is graphed as zero decibels. Thus, the OoB and spurious levels are graphed at relative power levels that are offset from absolute levels by two factors.

These are:

1) The difference between the graphed zero decibel (relative) power and the actual (absolute) power, $P_{transmit}$, at the fundamental; and
2) The decibel difference between the power measured at the transmitter's fundamental frequency or frequencies, f_0, in 1 MHz and the transmitter's full power that would have been measured in a sufficiently wide bandwidth to have convolved all of the transmitter's available power at f_0. This is power offset between power in 1 MHz and power in the full bandwidth of the transmitter is called $P_{BW\text{-}offset}$.

For radio transmitter modulations in which power in a bandwidth is directly proportional to the bandwidth, this variation will go as $10\log(B_{meas}/B_{transmitter})$,[15] where B_{meas} and $B_{transmitter}$ are the bandwidths of the measurement system and the transmitter, respectively.

The variable $P_{BW\text{-}offset}$ is defined as:

[15] This is true for LTE-type signal modulation that is RMS-detected. It is not true for radio signals in general. For example, for pulsed radar signals that are peak-detected the relationship goes as 20log of the bandwidth ratio at the radar f_0 and as about 15log of the bandwidth ratio in the radar OoB and spurious regions.

$P_{BW\text{-}offset} = 10\log(B_{meas}/B_{transmitter})$ for $B_{meas} \leq B_{transmitter}$ and

$P_{BW\text{-}offset} = 0$ for $B_{meas} > B_{transmitter}$.

Note that this factor is always less than or equal to zero.

Taking into these offsets on the relative-power data graphs, the suppression, S', to put on these graphs for the FCC mask limit must be

$$S' = L - P_{transmit} + P_{BW-offset} \tag{C-4}$$

or

$$S' = -13\frac{dBm}{MHz} - P_{transmit} + 10log\left(\frac{B_{meas}}{B_{transmitter}}\right). \tag{C-5}$$

For example, suppose that an eNB transmitter produced a total of +30 dBm of power in a 10 MHz bandwidth. In this case, S' would be

$$S' = -13\frac{dBm}{MHz} - 30\ dBm + 10\log\left(\frac{1\ MHz}{10\ MHz}\right) = -13 - 30 - 10 = -53\ dB. \tag{C-6}$$

The mask limit line would thus be drawn on the relative-data spectrum graph at at plotted power level, P_{plot}, of 53 dB below the zero-decibel power level (that is, at -53 dB on the plot) for the power measured in 1 MHz at the transmitter's fundamental frequency.

C.3.2. External Attenuation Considerations

A question to ask at this point is, what should be done about external attenuation of $A_{external}$ dB (e.g., 30 dB) in a high-power RF attenuator that might be (and in this study was) inserted between the transmitter (e.g., eNB) output port and the input of the measurement system to prevent overload of the measurement system? Unlike the built-in variable attenuation invoked by computer control within the measurement system's RF front end, this external attenuation was not automatically added back into the power measurement results as the measurement progressed (although its value was noted and documented by the measurement team). Should this attenuation be somehow included in the equation above? The answer is no. This is because, although the external attenuation reduced all parts of the measured spectrum by $A_{external}$ dB, it was in effect already added back into the measurement results when the subject spectra were normalized to zero decibels at the transmitter's fundamental frequency f_0. Having already been corrected in the normalization of the measured spectrum to zero decibels at f_0, there is no need for further correction when the emission mask limit is drawn.

C.3.3. Second Method for Plotting Absolute Masks on Hardline-Connected Relative Emission Spectra

There is a second way to solve the mask-limit drawing problem for hardline-coupled measurements such as were performed in this study on the eNB transmitter. That is to take advantage of the fact that the measurement system did record absolute measured power in the

subject bandwidth of 1 MHz on a frequency-by-frequency basis as the measurement progressed. Although those are data are not presented in absolute spectrum power density terms in this report, they do exist in the measurement team's original data files.[16]

For this approach, we do not need to know the power level at f_0. We need not have even measured power at f_0. But we do need to know every attenuation factor between the transmitter output and the detector in the measurement system. And we need to know what the bandwidth offset factor $P_{BW\text{-}offset}$ was. In this case, the mask limit is drawn relative to any one of the OoB or spurious data points. (Which point is chosen does not matter; the same math applies to every OoB and spurious point, and the mask limit across the spectrum will be a flat line, as we shall see.)

So, for an absolute measured power density power level, P_{meas},[17] when $A_{external}$ decibels of attenuation were between the transmitter and the measurement system RF front end input and the measurement system RF front end had $A_{internal}$ decibels of RF attenuation invoked, the mask will be drawn relative to P_{meas} by a number of decibels, Δ, as follows

$$\Delta = L - \left(P_{meas} + A_{external} + A_{internal} - P_{BW-offset}\right). \quad \text{(C-7)}$$

Since P_{meas} is subtracted in this equation to obtain Δ, it does not matter which value of P_{meas} (that is, which OoB or spurious data point) is selected to calculate Δ.

The power level at which the mask is drawn on a relative-power plot, P_{plot} is therefore

$$P_{plot} = P_{relative} + \Delta \quad \text{(C-8)}$$

where $P_{relative}$ is the power level of the selected OoB or spurious measurement point on the relative-power data plot.

For example, suppose that for a selected OoB or spurious point, P_{meas} = -65 dBm in 1 MHz measurement bandwidth, $A_{external}$ = 30 dB, $A_{internal}$ = 0 dB, $P_{BW\text{-}offset}$ = -10 dB, L = -13 dBm/MHz and $P_{relative}$ = -85 dB/MHz.

Then in this example,

$$P_{plot} = -85 + \left(-13 - (-65 + 30 + 0 - 10)\right) = -85 - 13 + 65 - 30 + 10 = -53\ dB. \quad \text{(C-9)}$$

This level for P_{plot} is the same as was calculated with the first method given above. The mask limit plotted-level results should of course always be the same for both of these methods.

[16] Those measured power densities are automatically stored in original measurement data files in two versions. In one version, the power levels have been corrected for the RF front end attenuation settings on a frequency-by-frequency basis. In the other version, the measured power levels have not had that correction applied. In neither case, however, have the data been corrected for the external attenuation of $A_{external}$ dB that was inserted in front of the RF front end, between the front end and the transmitter output.

[17] P_{meas} is assumed to have already been corrected for the measurement system's noise diode calibrated gain factor at the selected frequency.

C.3.4. Method for Plotting Absolute Masks on Radiatively Measured Relative Emission Spectra

The plotting problem might ostensibly appear to be more complicated for radiated emission spectrum measurements than for hardline measurements. This is because, for the radiated case, the measurement system can only convolve a fraction of the transmitter's power output. Furthermore, there is no reliable way to know what fraction of the transmitter's total power at its antenna input was radiated in the direction of, and coupled into, the measurement system antenna. But the solution is in fact as simple for radiated as for hardline connected measurements.

To solve this problem, we must know what the transmitter's rated mean maximum power, $P_{transmit}$, is supposed to be, as specified by for instance by the manufacturer. When we have this value[18] for $P_{transmit}$, we can solve the rest of the problem. The reason is that, whatever fraction of the transmitted power is captured by the measurement system, that fraction will be the same at all frequencies including f_0 and the OoB and spurious regions of the spectrum; the total fractional offset in decibels due to all antenna pattern and propagation factors will be identical across the entire spectrum (propagation loss being the same[19] at all frequencies in the anechoic measurement chamber that was used).

On the zero decibels at f_0 relative-power reference plots in this study, we can apply exactly the same equation as we did for the first method for hardline-coupled measurements to determine the level of P_{plot}

$$P_{plot} = S' = L - P_{transmit} + P_{BW-offset}. \quad \text{(C-10)}$$

For example, suppose that the FCC limit of -13 dBm/MHz is to be plotted for a UE that had a maximum rated output power of -23 dBm and which was operating with a 10 MHz f_0 bandwidth.

Then

$$P_{plot} = S' = -13\frac{dBm}{MHz} - 23\ dBm + 10log\left(\frac{1\ MHz}{10\ MHz}\right) = -46\ dB. \quad \text{(C-11)}$$

[18] If radiated measurements have been performed, as for the UEs in this study, because there is no hardline connection available by which to measure the transmitter's power, a manufacturer's specification or some equivalent engineering reference will be needed to establish the transmitter's mean maximum transmitter power output.

[19] It might be objected that free-space propagation is not the same at all frequencies; that propagation loss increases (and signal power therefore decreases) as 20log(frequency) according to various free-space propagation equations. As F. Sanders shows and explains in [11] however, the occurrence of the 20log(frequency) factor in such equations is unrelated to the propagation of energy in free space. Space treats all frequencies of electromagnetic radiation equally, with a frequency-invariant decrease (e.g., $1/r^2$ at all frequencies) as any wave front expands from a source. Put another way, the impedance of space is 377 ohms at all frequencies. The 20log factor is not an artifact of the behavior of space; it is rather an artifact of the conventional definition of an isotropic antenna. This artifact disappears for constant effective-aperture antennas such as parabolic dishes and horns, which have gain *relative to an isotropic reference antenna* that *increases* as 20log(frequency). Since the measurement antenna in this study was a horn, the 20log factor disappears from any calculations.

C.4. Non-FCC Absolute Emission Mask Limits

Non-FCC absolute power density emission mask limits have been defined for some systems by non-governmental organizations. The same methods as described above for plotting FCC limits on relative-power spectrum plots can be used for these other mask limits. Rather than setting the value of *L* at -13 dBm/MHz in the various equations, the alternative absolute spectrum power densities for other mask limits are used instead for *L*.

Abbreviations and Acronyms

3GPP	3rd Generation Partnership Project
AMT	Aeronautical Mobile Telemetry
AWS-3	Advanced Wireless Services version 3
CIO	Chief Information Officer
CPE	Consumer Premise Equipment
dB	Decibel
DoC	Department of Commerce
DoD	Department of Defense
DUT	Device Under Test
EIRP	Effective Isotropic Radiated Power
EMC	Electromagnetic Compatibility
eNB	Evolved Node B
ENR	Excess Noise Ratio
EPRE	Energy Per Resource Element
FCC	Federal Communications Commission
FDD	Frequency Domain Duplex
I	In-phase signal component
IF	Intermediate Frequency
IP	Internet Protocol
IRAC	Interdepartment Radio Advisory Committee
ITS	Institute for Telecommunication Sciences
LNA	Low Noise Amplifier
LTE	Long Term Evolution
MAC	Media Access Control
NASCTN	National Advanced Spectrum and Communications Test Network

NIST	National Institute of Standards and Technology
NTIA	National Telecommunications and Information Administration
OFDM	Orthogonal Frequency Division Multiplexed/Multiplexing
OoB	Out of Band
OSM	Office of Spectrum Management
PDCP	Packet Data Convergence Protocol
PUSCH	Physical Uplink Shared Channel
Q	Quadrature-phase signal component
QAM	Quadrature Amplitude Modulated/Modulation
QPSK	Quadrature Phase Shift Keyed/Keying
RB	Resource Block (in an LTE radio link)
RBW	Resolution Bandwidth
RF	Radio Frequency
RMS	Root Mean Square
RRC	Radio Resource Control
TBSI	Transfer Block Size Index
TS	Technical Specification
TSC	Technical Subcommittee (of the IRAC)
TTR	Test and Training Range
UE	User Equipment
UMTS	Universal Mobile Telecommunications System
UTRAN	Universal Terrestrial Radio Access Network
VSG	Vector Signal Generator
YIG	Yttrium Iron Garnet

REPORT DOCUMENTATION PAGE

Form Approved
OMB No. 0704-0188

The public reporting burden for this collection of information is estimated to average 1 hour per response, including the time for reviewing instructions, searching existing data sources, gathering and maintaining the data needed, and completing and reviewing the collection of information. Send comments regarding this burden estimate or any other aspect of this collection of information, including suggestions for reducing the burden, to Department of Defense, Washington Headquarters Services, Directorate for Information Operations and Reports (0704-0188), 1215 Jefferson Davis Highway, Suite 1204, Arlington, VA 22202-4302. Respondents should be aware that notwithstanding any other provision of law, no person shall be subject to any penalty for failing to comply with a collection of information if it does not display a currently valid OMB control number.
PLEASE DO NOT RETURN YOUR FORM TO THE ABOVE ADDRESS.

1. REPORT DATE *(DD-MM-YYYY)*	**2. REPORT TYPE**	**3. DATES COVERED** *(From - To)*
26-OCT-2017	Technical Report	N/A

4. TITLE AND SUBTITLE
Measured Emission Spectra of Selected AWS-3 LTE Transmitters

5a. CONTRACT NUMBER
F1S0AG7088G001

5b. GRANT NUMBER

5c. PROGRAM ELEMENT NUMBER

6. AUTHOR(S)
Michael Frey
Geoffrey Sanders
Jolene Splett
John Ladbury
Frank Sanders
Azizollah Kord
Ryan Jacobs

5d. PROJECT NUMBER
6817000-300

5e. TASK NUMBER

5f. WORK UNIT NUMBER

7. PERFORMING ORGANIZATION NAME(S) AND ADDRESS(ES)
National Telecommunications and Information Administration, Institute for Telecommunication Sciences
325 Broadway, MS NTIA/ITS.D
Boulder, CO 80305

8. PERFORMING ORGANIZATION REPORT NUMBER
NASCTN Report 4
NTIA Technical Report TR-18-528
NIST Technical Note TN 1980

9. SPONSORING/MONITORING AGENCY NAME(S) AND ADDRESS(ES)
412th Test Wing (AFMC)
Edwards Air Force Base, CA

10. SPONSOR/MONITOR'S ACRONYM(S)

11. SPONSOR/MONITOR'S REPORT NUMBER(S)

12. DISTRIBUTION/AVAILABILITY STATEMENT
Approved for Public Release. Distribution Unlimited.

13. SUPPLEMENTARY NOTES
This was a collaborative effort of the National Advanced Spectrum and Communications Test Network (NASCTN).

14. ABSTRACT
Version three of Advanced Wireless Services (AWS-3) radio systems will soon use spectrum that is adjacent to bands currently used by airborne telemetry links at U.S. government test and training ranges (TTRs). Out-of-band (OoB) and spurious emissions from AWS-3 base stations (within LTE these are referred to as evolved node Bs, or eNBs) and their associated mobile units (called user equipment or UEs) could cause interference to these adjacent-band telemetry receivers. Electromagnetic compatibility (EMC) analyses for such interference will rely on knowing the power spectra of the OoB and spurious emissions of AWS-3 eNBs and UEs over frequencies used by telemetry link receivers. To determine these power spectra, the authors have measured transmitter OoB and spurious emissions of an AWS-3 eNB and selected UEs. Adaptive power attenuation allowed these measurements to be made with over 100 decibels (dB) of dynamic range. The measurements have been collected in a variety of resolution bandwidths, transmitter modulations, and types of transmitter loading (i.e., number of resource blocks used) for two measurement detector modes. The results of those measurements are provided in this report. In general, AWS-3 eNB and UE transmitted emission spectra are found to be insensitive to variations in transmitter modulations and resource block configurations. The measured power spectra of the eNBs and UEs vary in direct proportion to measurement (or receiver) bandwidth (i.e., as 10 log measurement bandwidth) with an approximate offset of about 10 dB between peak and average levels. The measurement results indicate that AWS-3 eNB and UE power spectra were suppressed by at least 100 dB in the adjacent telemetry bands for the devices tested. The results can now be factored into EMC analyses for AWS-3 transmitters operating in proximity to telemetry receivers.

15. SUBJECT TERMS
1755-1780 MHz; 2155 – 2180 MHz; AWS-3; aeronautical mobile telemetry (AMT); Band 66; band sharing; band sharing analysis; emission spectrum; eNodeB (eNB); interference analysis; out of band (OoB) emissions; spectrum measurements; spectrum sharing; telemetry links; user equipment (UE)

16. SECURITY CLASSIFICATION OF:			**17. LIMITATION OF ABSTRACT**	**18. NUMBER OF PAGES**	**19a. NAME OF RESPONSIBLE PERSON**
a. REPORT	**b. ABSTRACT**	**c. THIS PAGE**			Sheryl Genco, Acting NASCTN Program Manager
Unclassified	Unclassified	Unclassified	Same as Report	68	**19b. TELEPHONE NUMBER** *(Include area code)* 303-497-3591